Burns & Trauma, 2023, 11, tkad034
https://doi.org/10.1093/burnst/tkad034
Research Article

OXFORD

Research Article

Extracellular vesicles from 3D cultured dermal papilla cells improve wound healing via Krüppel-like factor 4/vascular endothelial growth factor A -driven angiogenesis

Yunwei Wang[1,†], Kuo Shen[1,†], Yulin Sun[2,†], Peng Cao[3,†], Jia Zhang[4], Wanfu Zhang[1], Yang Liu[1], Hao Zhang[1], Yang Chen[1], Shaohui Li[1], Chaolei Xu[1], Chao Han[1], Yating Qiao[5], Qingyi Zhang[1], Bin Wang[1], Liang Luo[1,*], Yunshu Yang[1,*] and Hao Guan[1,*]

[1]Department of Burns and Cutaneous Surgery, Xijing Hospital, Fourth Military Medical University, 127 West Changle Road, Xi'an, 710032, China, [2]Department of Plastic Surgery, Shanghai East Hospital, Tongji University School of Medicine, 150 Jimo Road, Shanghai, 200120, China, [3]Department of Burns and Plastic Surgery, General Hospital of Ningxia Medical University, 804 South Shengli Street, Yinchuan, 750004, China, [4]Department of Dermatology, Xijing Hospital, Fourth Military Medical University, 127 West Changle Road, Xi'an, 710032, China and [5]Department of hair diagnosis and treatment, Peking University Shougang Hospital, 9 Jinyuanzhuang Road, Beijing, 100144, China

*Correspondence. Liang Luo, Email:clayluo@outlook.com; Yunshu Yang, Email:yangys0815@qq.com; Hao Guan, Email:guanhao2020@yeah.net

[†]These authors contributed equally to this work.

Received 3 March 2023; Revised 13 April 2023; Accepted 19 May 2023

Abstract

Background: Non-healing wounds are an intractable problem of major clinical relevance. Evidence has shown that dermal papilla cells (DPCs) may regulate the wound-healing process by secreting extracellular vesicles (EVs). However, low isolation efficiency and restricted cell viability hinder the applications of DPC-EVs in wound healing. In this study, we aimed to develop novel 3D-DPC spheroids (tdDPCs) based on self-feeder 3D culture and to evaluate the roles of tdDPC-EVs in stimulating angiogenesis and skin wound healing.

Methods: To address the current limitations of DPC-EVs, we previously developed a self-feeder 3D culture method to construct tdDPCs. DPCs and tdDPCs were identified using immunofluorescence staining and flow cytometry. Subsequently, we extracted EVs from the cells and compared the effects of DPC-EVs and tdDPC-EVs on human umbilical vein endothelial cells (HUVECs) *in vitro* using immunofluorescence staining, a scratch-wound assay and a Transwell assay. We simultaneously established a murine model of full-thickness skin injury and evaluated the effects of DPC-EVs and tdDPC-EVs on wound-healing efficiency *in vivo* using laser Doppler, as well as hematoxylin and eosin, Masson, CD31 and α-SMA staining. To elucidate the underlying mechanism, we conducted RNA sequencing (RNA-seq) of tdDPC-EV- and phosphate-buffered saline-treated HUVECs. To validate the RNA-seq data, we constructed knockdown and overexpression vectors of Krüppel-like factor 4 (KLF4). Western blotting, a scratch-wound assay, a Transwell assay and a tubule-formation test were performed to detect the protein expression, cell migration and lumen-formation ability of KLF4 and vascular endothelial growth factor A (VEGFA) in HUVECs incubated with tdDPC-EVs after KLF4 knockdown or overexpression. Dual-luciferase reporter gene assays were conducted to verify the activation effect of KLF4 on VEGFA.

Results: We successfully cultured tdDPCs and extracted EVs from DPCs and tdDPCs. The tdDPC-EVs significantly promoted the proliferation, lumen formation and migration of HUVECs. Unlike DPC-EVs, tdDPC-EVs exhibited significant advantages in terms of promoting angiogenesis, accelerating wound healing and enhancing wound-healing efficiency both *in vitro* and *in vivo*. Bioinformatics analysis and further functional experiments verified that the tdDPC-EV-regulated KLF4/VEGFA axis is pivotal in accelerating wound healing.

Conclusions: 3D cultivation can be utilized as an innovative optimization strategy to effectively develop DPC-derived EVs for the treatment of skin wounds. tdDPC-EVs significantly enhance wound healing via KLF4/VEGFA-driven angiogenesis.

Graphical Abstract

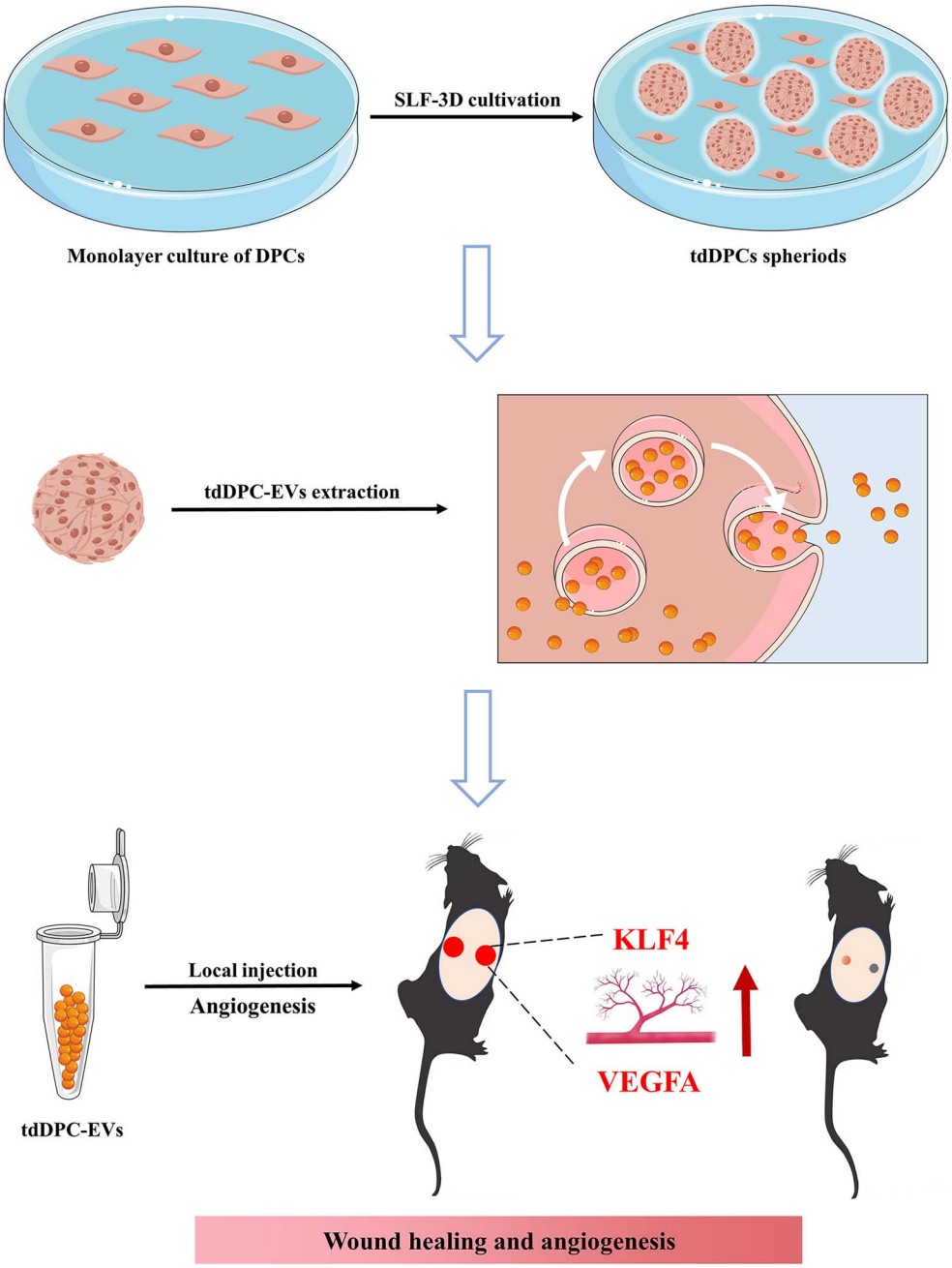

Key words: Extracellular vesicles, Dermal papilla cells, 3D spheroids, Wound healing, Angiogenesis

Background

The skin wound-healing process is characterized by the well-orchestrated integration of several factors, including the cooperation of various cell types and their derivative molecules, and is underpinned by cell proliferation, adhesion and migration [1]. The angiogenic response was one of the first processes identified as essential for wound repair [2]. Upon tissue injury, vascular structure destruction leads to hypoxia. The recovery of the normal oxygen content is essential to boost skin cell proliferation, wound epithelialization and hair follicle regeneration. During wound healing, the new capillary bed undergoes remodeling and maturation. Many poorly healed wounds, especially those with full-thickness skin defects, often show abnormal angiogenesis, such as capillary overgrowth and poor mature blood vessel formation, ultimately leading to scar formation [3]. Scars not only affect the appearance of individuals but also cause a lack of skin appendages, excessive collagen deposition, disordered fiber arrangement, and poor tissue ductility and tension resistance, which seriously affect the patient's quality of life. Despite advances in current wound-treatment strategies, therapeutic approaches to improve wound-healing efficiency require further improvement. Therefore, regulating wound capillary regeneration is a quintessential therapeutic goal.

Several reports have highlighted mesenchymal stem cells (MSCs) as promising wound-healing candidates owing to their remarkable potential to promote tissue repair and regeneration [4,5]. Furthermore, MSC-derived extracellular vesicles (EVs) hold promise for wound healing and tissue regeneration. Additionally, this cell-free treatment effectively circumvents the tumorigenicity associated with MSC transplantation and is convenient for application and storage [4]. Dermal papilla cells (DPCs), a specialized type of MSC that reside in the base of hair follicles (HFs) [6], play a pivotal role in epithelial–mesenchymal transition [7,8], HF regeneration and the *de novo* formation of HFs [9,10]. When skin is injured, DPCs can differentiate into dermal fibroblasts, contributing to wound repair [11]. Furthermore, DPCs are conducive to maintaining the viability of progenitor populations within the epidermis, promoting early neovascularization and alleviating local inflammation during wound healing [12]. In addition, several growth factors and cytokines secreted by DPCs regulate cell proliferation, HF development and angiogenesis [13]. For instance, DPC-released vascular endothelial growth factor (VEGF) and insulin-like growth factor 1 (IGF-1) promote the maturation, proliferation and lumen-formation capacity of human microvascular endothelial cells [14]. Moreover, the paracrine effect of DPCs may contribute to wound healing. Several studies have extended the theoretical basis for applying DPC-EVs for hair regeneration and skin damage repair [15–17]. However, owing to the lack of a suitable environment for epithelial–mesenchymal transition, the biological activity of isolated primary DPCs is gradually lost during traditional 2D long-term subculture *in vitro* [18–20]. Generally, DPCs beyond the sixth generation show evident morphological changes, such as no longer exhibiting aggregate growth. Compared with that of DPCs below the sixth generation, the vitality of high-passage cells decreases significantly, markedly limiting advances in the application of DPCs for wound healing.

3D cell culture, an important method to promote cell proliferation and function, is a promising therapeutic method for addressing the aforementioned issues [21,22]. In 2007, through the study of the characteristic recovery of DPCs cultured *in vitro*, Osada [23] found that the 3D culture of DPCs could partially simulate the complete dermal papilla and preserve the hair induction ability of DPCs. Compared with those of 2D-cultured DPCs, the biological characteristics and function of DPCs in 3D culture conditions were significantly enhanced. Research also showed that compared with 2D MSCs, 3D MSC spheroids have significantly enhanced allomeric function, exhibiting higher EV secretion, smaller EV sizes, and higher cytokine and mediator secretion [24,25].

Currently, 3D cell culture techniques mainly comprise scaffold-based and scaffold-free structures [26]. Among them, the hanging-drop method and low-adhesion technology are widely implemented. However, the aforementioned culture methods still have limitations in clinical applications because cell proliferation in the sphere slows down, the central cell mass of the sphere is prone to hypoxia and necrosis, and the yield is low during long-term culture [27,28]. Our previous research demonstrated that low concentrations of fetal bovine serum (FBS) and growth factors, including basic fibroblast growth factor (bFGF), epidermal growth factor (EGF) and platelet-derived growth factor (PDGF), could induce MSCs to form 3D spheroids spontaneously on a specific matrix scaffold. The spheroids of human adipose-derived MSCs that formed on the self-feeder 3D (SLF-3D) exhibited stemness and multilineage differentiation potential [29,30]. However, there are few studies on the application of DPC-EVs in wound treatment, and the role of 3D-DPC-EVs in promoting wound healing and scar treatment has not been reported.

Here, we aimed to create novel 3D-DPC spheroids (tdDPCs) based on SLF-3D culture. Furthermore, the capacity of DPC-EVs and tdDPC-EVs to stimulate angiogenesis during wound healing was also evaluated. Moreover, we studied the underlying mechanisms of tdDPC-EVs action by treating human umbilical vein endothelial cells (HUVECs) with DPC-EVs and tdDPC-EVs, respectively, and subjecting them to RNA-sequencing (RNA-seq). Overall, we anticipate that 3D culture can be utilized as a simple and innovative optimization strategy for using DPC-derived EVs to treat wounds, thereby satisfying current clinical demands.

Methods

Antibodies

The following antibodies were used in this study: anti-lymphoid enhancer-binding factor 1 (anti-LEF1) (2230, Cell Signaling Technology; 1 : 200), anti-alkaline phosphatase (anti-ALP) (AF2910, R&D System; 1 : 500), anti-Ki67

(SAB5700770, Sigma; 1 : 100), anti-CD31 (GB11063–2, Servicebio, China; 1 : 400), anti-α-SMA (ab124964, Abcam; 1 : 200), anti-calnexin (ab22595, Abcam; 1 : 1000), anti-TSG101 (ab125011, Abcam; 1 : 1000), anti-CD9 (ab92726, Abcam; 1 : 1000), anti-CD81 (ab109201, Abcam; 1 : 1000), anti-Krüppel-like factor 4 (anti-KLF4) (ab214666, Abcam; 1 : 1000), anti-VEGFA (ab214424, Abcam; 1 : 1000), HRP-conjugated goat anti-rabbit IgG (D110058, Sangon Biotech, China; 1 : 3000), DyLight 488-conjugated AffiniPure rabbit anti-goat IgG (BA1124, BOSTER, China; 1 : 200) and DyLight 594-conjugated AffiniPure goat anti-rabbit IgG (BA1127, BOSTER; 1 : 200).

Isolation, culture and identification of DPCs and tdDPCs

Primary DPCs were derived from the dermal papilla of whisker pads from 6-week-old C57BL/6 male mice, as previously described [31]. In short, the whisker HFs were extracted from the dermis, whereafter the end bulbs were cut off from the hair shafts and transferred to a sterile Petri dish containing high-glucose Dulbecco's modified Eagle's medium (DMEM, SH30022.01, Hyclone) supplemented with 20% FBS (Biological Industries). Primary DPCs at passages 1–5 were cultured in high-glucose DMEM with 10% FBS at 37°C with 5% CO_2 in a humidified atmosphere. After five passages, DPCs were cultured in DMEM/nutrient mixture F-12 (DMEM/F-12, 12 660 012, Gibco) with 10% FBS. Primary DPCs were dissociated using incubation with StemPro™ Accutase™ Reagent (A1110501, Gibco) for 5 min, and then used to prepare a single-cell suspension that was seeded at a density of 5×10^4 cells/cm^2 in a 3D culture medium containing 2% FBS, human bFGF (5 ng/ml, Peprotech), human EGF(2 ng/ml, Peprotech), human PDGF (5 ng/ml, Peprotech), heparin (2 μg/ml, Sigma, Mississauga, ON, USA), L-ascorbic acid 2-phosphate sesquimagnesium salt hydrate (50 μg/ml, Sigma), 100 units/ml penicillin and 100 μg/ml streptomycin for >5 days, as previously described by our group [30]. After DPCs grew to 90–100% confluency, semi-suspended spheroids were formed on the attached DPCs, which are referred to as tdDPCs. When the spheroids grew to a density of 10/cm^2, vigorous shaking and centrifugation were applied to collect primary spheroids. Primary tdDPC spheroids were detached into single tdDPCs using StemPro™ Accutase™ Reagent for 5 min, followed by another passage. Single tdDPCs were replated into the original flasks, where some attached DPCs remained as scaffolds; these tdDPCs formed semi-suspended 3D spheroids again following culture for 3–5 days and are referred to as secondary tdDPCs. Each passage included the above procedures. During follow-up cultures and passages, tdDPCs exhibited stable proliferation and passage characteristics in the standard DMEM/F-12 medium containing 10% FBS. DPCs and tdDPCs were identified according to a previously reported method [32,33]. Specifically, cells were seeded into 24-well plates, covered with glass coverslips, at 10–20% confluence. Cells that adhered to the glass were washed twice with phosphate-buffered saline (PBS), fixed with 4% paraformaldehyde, permeabilized with 0.1% Triton X-100 and blocked in 4% bovine serum albumin (BSA). The cells were incubated with LEF1 (1 : 100) and ALP (1 : 100) antibodies overnight at 4°C, incubated with fluorescence-conjugated secondary antibodies for 1 h the next day and mounted with DAPI Fluoromount-G (0100–20, SouthernBiotech, USA). Slides were observed under an EVOS™ FL Auto 2 microscope (AMAFD2000, Invitrogen, USA).

For the flow cytometric analysis of surface markers, both DPCs and tdDPCs were incubated with PE-conjugated anti-CD29 (112 207, eBioscience, USA; 1 : 20), PE-conjugated anti-CD34 (800 504, BioLegend, USA; 1 : 20), PE-conjugated anti-CD44 (103 007, BioLegend; 1 : 20), PE-conjugated anti-CD90 (140 307, BioLegend; 1 : 20), PE-conjugated anti-CD105 (120 407, BioLegend; 1 : 20) and FITC-conjugated anti-CD45 (157 213, BioLegend; 1 : 20) antibodies for 30 min at 4°C. The percentages of positively stained cells were determined using a Coulter Epics XL flow cytometer (Beckman Coulter, USA) and EXPO32 ADC Analysis software (Beckman Coulter).

To identify adipogenic and osteogenic differentiation, ~80–90% confluent cells were imaged under an Olympus IX71 light microscope (Olympus, Japan).

Isolation and characterization of EVs

After primary DPCs and tdDPCs were cultured in a medium with 10% EV-depleted FBS for 24 h, EVs were isolated from the supernatant using differential ultracentrifugation, as previously described [15]. DPC-EVs and tdDPC-EVs were then quantified using a Pierce BCA Protein Assay Kit (Thermo Fisher Scientific, Waltham, MA, USA) at 562 nm. EV surface marker expression was analyzed using western blotting with the previously indicated primary antibodies. EV morphology was observed via transmission electron microscopy (TEM; HT-7700, Hitachi, Japan). The morphology and size distribution of DPC-EVs and tdDPC-EVs were determined via NanoFCM, as previously described [24]. A PKH26 red fluorescent cell linker kit (PKH26PCL, Sigma) was used to label DPC-EVs and tdDPC-EVs. The PKH26-labeled DPC-EVs and tdDPC-EVs were incubated with HUVECs for 24 h. The cells were then fixed in 4% paraformaldehyde for 30 min, stained with DAPI (D9542-1MG, Sigma-Aldrich; 1 μg/ml) and photographed under an EVOS™ FL Auto 2 microscope.

Cell cultures

Primary HUVECs were acquired from the Department of Ophthalmology, Xijing Hospital, Fourth Military Medical University and cultured in endothelial cell medium (1001, ScienCell) containing 1% endothelial cell growth supplement (1052, ScienCell).

Simultaneously, 10 μg/ml DPC-EVs, tdDPC-EVs and the same amount of PBS were added to the culture medium of HUVECs according to the different treatment groups.

Cell proliferation assay

HUVECs were seeded into 96-well plates (5×10^3/well), cultured in EV-free low-serum (2% FBS), and treated with PBS, DPC-EVs or tdDPC-EVs (10 μg/ml). At 0, 12, 24, 36, 48 and 60 h, CCK-8 (C0038, Beyotime, China) was added to each culture medium (100 μl per well). Four repeated measurement wells were set up for each time point. After incubation at 37°C for 2 h, the absorbance was measured at 450 nm to detect cell proliferation changes.

HUVECs were seeded in 24-well culture plates and immunofluorescence-stained on chamber slides. After being treated with PBS, DPC-EVs or tdDPC-EVs (10 μg/ml), the cells were fixed with 4% cold paraformaldehyde for 15 min, immersed in 0.25% Triton X-100 for 5 min, blocked with 1% BSA for 30 min and incubated with anti-Ki67 (1 : 100) for 12 h at 4°C. After washing three times with PBS, the cells were incubated using fluorescein-conjugated secondary antibodies (1 : 200 in 1% BSA, Proteintech) for 30 min at 25°C. Following DAPI staining for 5 min to counterstain cell nuclei, the cells were photographed under the EVOS™ FL Auto 2 microscope.

Cell migration assay

For Transwell assays, $\sim 5 \times 10^4$ HUVECs suspended in FBS-free medium were inoculated in the upper chambers of Transwell 24-well plates (3422, Corning, USA). The lower chambers were filled with 600 μl of EV-free and endothelial cell growth supplement-depleted medium (5% FBS) as nutritional attractants, with or without EVs (10 μg/ml). After 12 h of culture, the cells were washed in PBS three times, fixed in 4% paraformaldehyde for 30 min and stained with 0.5% crystal violet for 30 min. Non-invasive or non-migrated cells were removed using clean cotton swabs. Five visual fields for each well were randomly photographed under a bright field microscope.

For scratch-wound-healing assays, HUVECs were inoculated into 6-well culture plates. A sterile 200 μl pipette tip was used to scratch the surface of cells at a confluence of 90–100%, in the shape of a cross. PBS was used to remove floating cells, and FBS-free medium, with or without EVs (10 μg/ml), was added. The scratches were photographed at 0, 12 and 24 h under an inverted microscope (Zeiss, Germany).

Lumen-formation assay

Matrigel Matrix (200 μl/well; 1 : 1, BD Biosciences) was added onto 48-well plates at 37°C for 30 min. HUVECs (1×10^5/well) suspended in 200 μl of FBS-free endothelial cell medium were inoculated onto polymerized Matrigel, with or without EVs (10 μg/ml). After incubation at 37°C for 3 and 6 h, tube formation was examined under the EVOS™ FL Auto 2 microscope. This experiment was performed three times for each condition. Image J software was utilized to analyze the capillary length and branch points.

Animal model

A total of 15 healthy, 6-week-old male C57BL/6 mice were purchased from the Experimental Animal Center of the Fourth Military Medical University. All procedures were approved by the Ethics Committee of the Fourth Military Medical University.

Two full-thickness skin wounds (5 mm in diameter) were made with a surgical perforator on either side of the spine after removing the hair from the backs of mice. Model mice were randomly and equally assigned to three treatment groups using a randomized digital table (PBS, DPC-EVs and tdDPC-EVs) and were subcutaneously injected around the wound with PBS, DPC-EVs (50 μg in 100 μl of PBS) or tdDPC-EVs (50 μg in 100 μl of PBS) on days 0–2 (Figure 6a). The wounds and blood perfusion were evaluated on days 0, 7 and 14, and were photographed using a Specimen Imaging System (RuiFeng Instrument, China). Mice were sacrificed on day 14 to collect tissues for subsequent experiments.

Wound healing

Image J software was used to analyze and quantify the wound area. The wound healing rate (WHR) was calculated as follows: WHR = $[(A_0—A_t)/A_0] \times 100\%$, where A_0 indicates the initial wound diameter on day 0 and A_t refers to the wound diameter at the indicated time point.

Wound blood perfusion imaging and assessment

Blood flow to the wounds and their surrounding area was detected using a laser Doppler perfusion imaging analyzer (Perimed AB, Sweden). A laser Doppler was fixed at a standard distance of 8–10 cm from the wound. The perfusion in the wound area (ROI 1) and the adjacent skin was detected at a distance from the wound border (ROI 2). The average blood perfusion rate (BPR) was calculated as follows: BPR = ROI 1/ROI 2.

Hematoxylin and eosin (H&E) and Masson staining

Mouse skin wound tissues were fixed in 4% paraformaldehyde, embedded in paraffin, and cut into 4-μm-thick sections. The sections were stained with H&E or Masson's trichrome and imaged under a PANNORAMIC 250 Flash series digital scanner (3DHISTECH, Hungary).

RNA extraction and quantitative reverse transcription-polymerase chain reaction analysis

Total RNA was extracted from HUVECs using TRIzol reagent (9109, Takara, Japan) and 1 μg of RNA was reverse-transcribed into cDNA using the Prime Script™ RT Reagent Kit (RR036A-1, Takara). Quantitative reverse transcription-polymerase chain reaction (qRT-PCR) was performed using UltraSYBR Mixture (CW0957M, CWBIO, China) and specific primers for each gene. β-Actin served as the housekeeping gene. The primers used are as follows: *KLF4*, forward: 5′-GGCGAGTCTGACATGGCTG-3′; *KLF4*, reverse: 5′-GCTGGACGCAGTGTCTTCTC-3′; *VEGFA*, forward: 5′-AGGGCAGAATCATCACGAAGT-3′; *VEGFA*, reverse: 5′-AGGGTCTCGATTGGATGGCA-3′; β-a*ctin*, forward: 5′-CTCCATCCTGGCCTCGCTGT-3′; β-a*ctin*, reverse: 5′-GCTGTCACCTTCACCGTTCC-3′.

RNA-sequencing

Total RNA from tdDPC-EV- or PBS-treated HUVECs was extracted using TRIzol reagent (Takara) and purified using Dynabeads™ Oligo(dT)25 (Invitrogen, Carlsbad, CA, USA). Using the same method, the total RNA of DPC-EVs and tdDPC-EVs was extracted. A cDNA library for sequencing was constructed using the NEB kit (7530, New England Biolabs). Transcriptome sequencing based on the Illumina HiSeq Xten system and related bioinformatic analyses were performed using OmicShare (https://www.omicshare.com/tools) by Gene Denovo Biotechnology Co. (Guangzhou, China). Expression levels of genes in each sample were normalized to fragments per kilobase of transcript per million mapped reads (FPKM). The DEseq2 [34] algorithm was applied to filter differentially expressed genes (DEGs) and statistical significance was defined by an FDR-adjusted p-value of <0.05 and $|\log_2 FC| > 2$.

Protein extraction and western blotting

Cell pellets and EVs were lysed in radioimmunoprecipitation assay buffer with 1× protease inhibitor cocktail (HY-K0010, MedChemExpress). Protein concentrations were measured using a BCA kit (P0012, Beyotime). Equal amounts of protein were separated via sodium dodecyl-sulfate polyacrylamide gel electrophoresis, transferred onto a polyvinylidene difluoride membrane (IPVH00010, Millipore, USA) and incubated with primary antibodies overnight at 4°C. The membrane was then incubated with HRP-conjugated secondary antibodies on the next day. Protein expression was visualized using ECL substrate (WBKLS0050, Millipore).

Luciferase assay

To determine the transcriptional regulation of KLF4 at the VEGFA promotor, plasmids encoding 2000 bp of wild-type promotor sequence, named h-VEGFA-pro, and a mutated KLF4-binding site, named h-VEGFA-mut, were used; pGL3-Basic served as the negative control. HUVECs were seeded in 96-well culture plates (1×10^4 cells/well). After 48 h of co-transfection of KLF4 overexpression plasmids and the above reporter constructs, the Promega Dual-Luciferase system (Promega, #E1910) was used to detect reporter activity. Luciferase activity was normalized to Renilla luciferase activity.

Statistical analysis

All data were statistically analyzed using GraphPad Prism 9. The t-test was used to compare two groups of data, two-way repeated measurement analysis of variance (ANOVA) was used for three groups of data affected by time, and one-way ANOVA was used for three groups of data unaffected by time. The Dunnett t-test was applied as the *post hoc* test after ANOVA. The results are presented as means ± standard deviation (SD). The statistical significance of differences was calculated using ANOVA and $p < 0.05$ indicated statistical significance.

Results

Isolation and identification of DPCs and tdDPCs

DPCs extracted from whisker HFs were readily visible around the condensates on day 5 (Figure 1a). Primary DPCs at passage 3 cultured in a 2D monolayer were spindle-shaped in appearance (Figure 1b). We previously developed a novel and economical SLF-3D adipose stem cell culture method [29], which we applied to culture primary DPCs in the 3D-specific conditioned medium for >5 days. The abundant tdDPCs were semi-suspended on the SLF-3D (Figure 1b). In order to further identify DPCs and tdDPCs, specific markers such as ALP and LEF1 were detected using immunofluorescence double-label staining. Both ALP and LEF1 were expressed in DPCs and tdDPCs (Figure 1c). Moreover, to identify DPCs and tdDPCs, we detected stem cell and dermal papilla cell marker proteins using flow cytometry and immunofluorescence staining. The results showed that DPCs and tdDPCs expressed CD29, CD44, CD90 and CD105, and that their expression in tdDPCs was higher; neither cell type expressed CD34 and CD45 (Figure 2).

Characterization of DPC-EVs and tdDPC-EVs

DPC-EVs and tdDPC-EVs were identified via TEM, western blotting and NanoFCM (Figure 3). TEM was used to observe the morphology of DPC-EVs and tdDPC-EVs and revealed a spherical or biconcave-disk shape (Figure 3a). Further, both DPC-EVs and tdDPC-EVs expressed the EV-specific surface marker proteins TSG101, CD81 or CD9, but were negative for calnexin expression (Figure 3b). Particle size analysis indicated that DPC-EVs and tdDPC-EVs had average particle sizes of 148.80 and 77.44 nm, respectively (Figure 3c). The concentrations of isolated DPC-EVs and tdDPC-EVs were 5.26×10^9 and 3.14×10^{10} particles/ml, respectively. The average particle size of tdDPC-EVs was smaller than that of DPC-EVs, and the particle concentration was higher (~6-fold).

tdDPC-EVs more effectively promote HUVEC proliferation than DPC-EVs

As angiogenesis can promote wound healing, we investigated the effects of tdDPC-EVs and DPC-EVs on angiogenesis by performing immunofluorescence staining and CCK8 assays to detect the proliferation of endothelial cells. First, we utilized PKH26 to label DPC-EVs and tdDPC-EVs. Fluorescence microscopy revealed the uptake of PKH26-labeled DPC-EVs and tdDPC-EVs by HUVECs (Figure 4a), indicating that the EVs present in DPCs or tdDPCs were internalized. We then evaluated the effects of the different treatments on the proliferation of HUVECs using CCK-8 assays (Figure 4b). Moreover, we also performed immunofluorescence staining

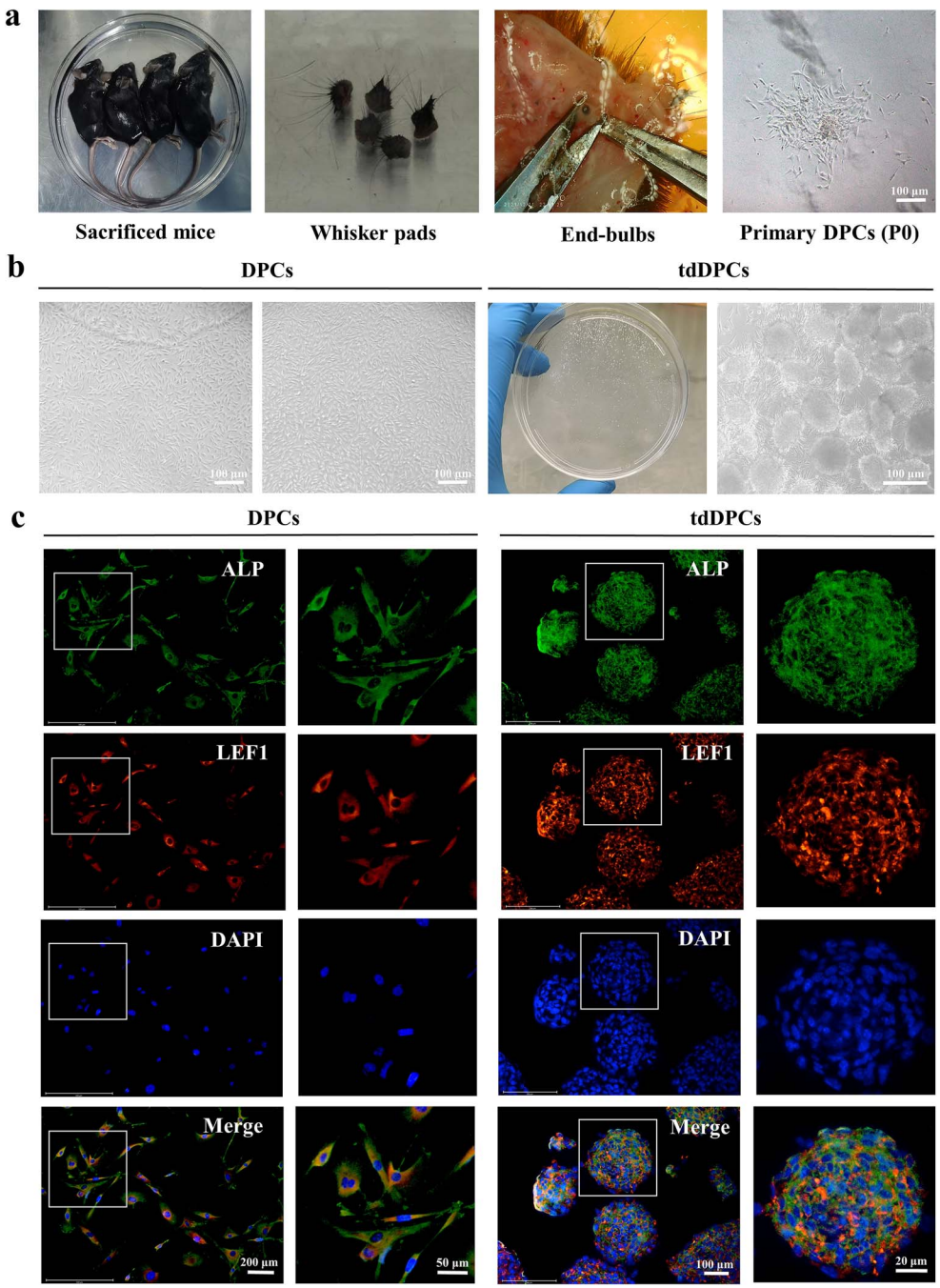

Figure 1. Isolation and identification of primary hair follicle dermal papilla cell (DPC) and 3D dermal papilla cell (tdDPC). (**a**) Photographs showing primary DPC isolation, including dissection of whisker pads, end-bulb isolation and DPC extraction. Scale bar: 100 μm. (**b**) Cellular morphology of DPC and tdDPC cultures (3D spheroids). Scale bar: 100 μm. (**c**) Immunofluorescence analysis of alkaline phosphatase (ALP) and lymphoid enhancer-binding factor 1 (LEF1) as specific markers of DPCs or tdDPCs. Scale bars: 20–200 μm

for Ki67, which indicated that tdDPC-EVs visibly enhanced the proliferation of HUVECs to a greater extent than both DPC-EVs and PBS (Figure 4c). We subsequently performed statistical analysis of the results of Ki67 fluorescence staining (Figure 4d), which indicated that tdDPC-EVs enhanced the proliferation of HUVECs more potently than DPC-EVs.

tdDPC-EVs exert greater pro-angiogenic effects on HUVECs than DPC-EVs

Scratch-wound and Transwell assays were then performed to evaluate the migration of HUVECs. Despite the significantly enhanced migration observed under DPC-EV treatment compared with that under PBS treatment, tdDPC-EVs further

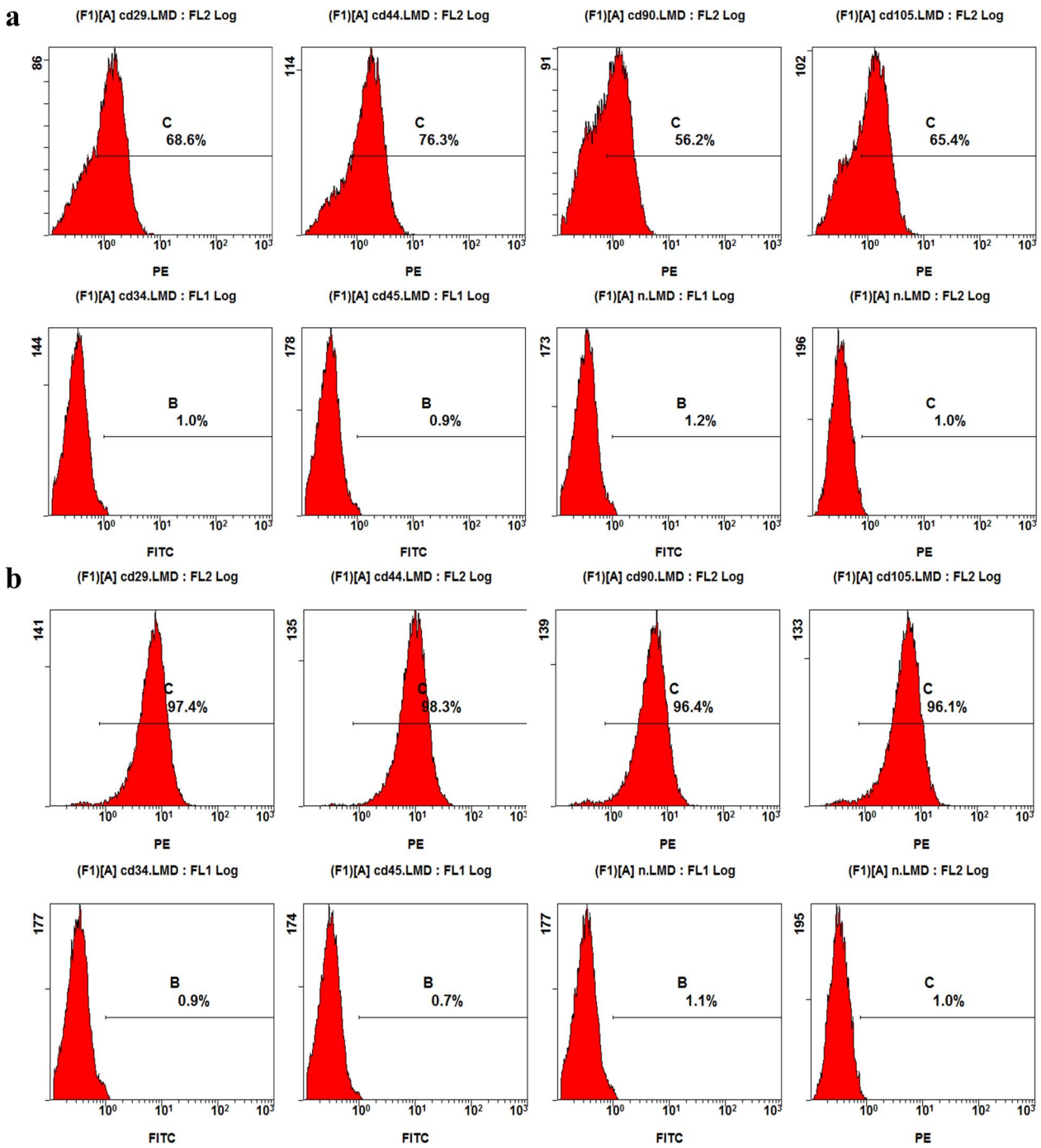

Figure 2. Characterization of stem cell markers in dermal papilla cells (DPCs) and 3D dermal papilla cell (tdDPCs). Flow cytometry results showed that DPCs (**a**) expressed CD29 (68.60%), CD44 (76.30%), CD90 (56.20%), and CD105 (65.40%) and tdDPCs (**b**) expressed CD29 (97.40%), CD44 (98.30%), CD90 (96.40%), and CD105 (96.10%); the expression was higher in tdDPCs (b), while neither cell type expressed CD34 and CD45, and the positive cell expression rate was less than or equal to 1%. *PE* phycoerythrin, *FITC* fluorescein isothiocyanate

enhanced HUVEC migration (Figure 5a, b). Similar results were obtained in tube-formation assays (Figure 5c). Collectively, these findings suggest that tdDPC-EVs have greater pro-angiogenic effects on HUVECs than DPC-EVs.

tdDPC-EVs enhance wound-healing efficiency and speed in mice

To determine the effects of DPC-EVs and tdDPC-EVs on wound healing *in vivo*, full-thickness skin defect wounds were

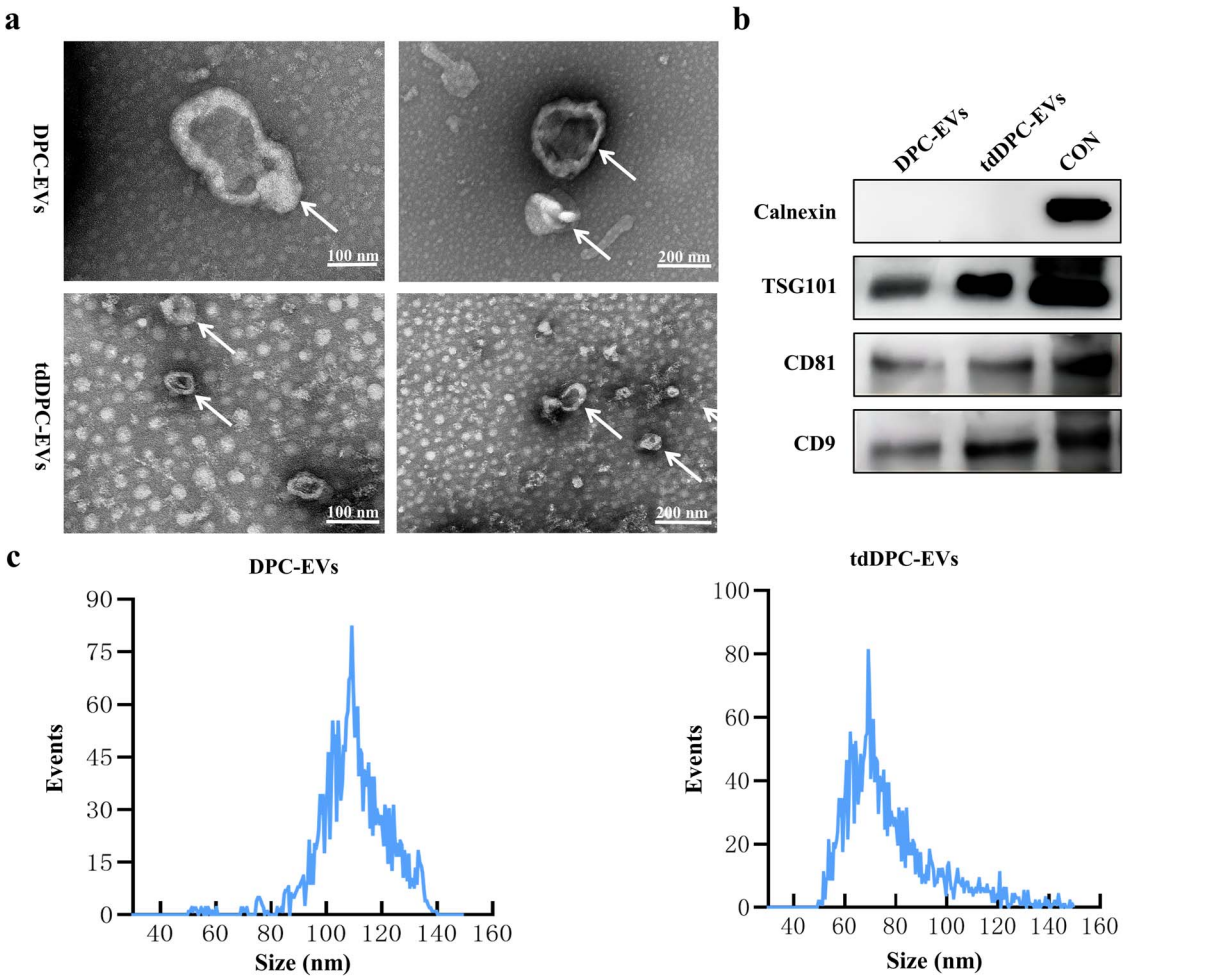

Figure 3. Characterization of dermal papilla cell extracellular vesicles (DPC-EVs) and 3D dermal papilla cell extracellular vesicles (tdDPC-EVs). (**a**) Ultrastructure of DPC-EVs and tdDPC-EVs, visualized via transmission electron microscopy (TEM). Scale bar: 100 or 200 nm. (**b**) Western blot analysis for EV markers TSG101, calnexin, CD81 and CD9. 293 T cell lysates were used as a control (CON). Particle size distribution of (**c**) DPC-EVs and (**d**) tdDPC-EVs, determined using NanoFCM

made on the shaved backs of mice, and tdDPC-EVs, DPC-EVs or PBS was injected subcutaneously around the wounds at days 0–2 (Figure 6a). At 14 days after wounding, the tdDPC-EV treatment group exhibited significantly improved healing compared to the DPC-EV or PBS treatment groups (Figure 6b). On day 7, tdDPC-EV-treated wounds had epithelialized to a much greater extent than DPC-EV- or PBS-treated wounds (Figure 6c). Assessment of blood perfusion using Doppler signals detected within the wound margin during wound healing revealed that, despite the significant increment of blood perfusion in the DPC-EV group compared with that in the PBS group, tdDPC-EVs noticeably enhanced wound blood flow compared with DPC-EVs (Figure 6d). To examine the morphological differences during skin regeneration, H&E staining of wound tissues was performed on day 14, revealing that tdDPC-EVs drastically improved the speed and quality of wound healing, as evidenced by integrated epithelization, an improved homogeneous thickness and a massive increase in palingenetic cutaneous appendages in the dermis, compared with DPC-EVs and PBS. Masson staining revealed compact wavy collagen fibers in a disordered arrangement in the wounds of DPC-EV- and PBS-treated mice, while tdDPC-EVs improved collagen alignment, as indicated by the relatively loose and ordered collagen deposition (Figure 6e). Considering the apparent improvement of wound perfusion by tdDPC-EV treatment, we conducted immunofluorescence analysis of the endothelial marker CD31 and the mature vascular marker α-SMA in tissue sections obtained on day 14 to evaluate angiogenesis. In tdDPC-EV-treated wounds, more mature, larger vessels with thicker walls were observed, while wounds in the DPC-EV or PBS groups were covered with many capillaries (Figure 6f). Taken together, these results indicate that tdDPC-EVs are more effective in accelerating and improving wound healing than DPC-EVs and PBS.

KLF4/VEGFA signaling may underlie the remarkable pro-angiogenic effect of tdDPC-EVs

To determine the mechanism underlying tdDPC-EV-mediated regulation of angiogenesis during wound healing, we conducted transcriptome sequencing of HUVECs treated with tdDPCs or PBS. A total of 655 significant DEGs were

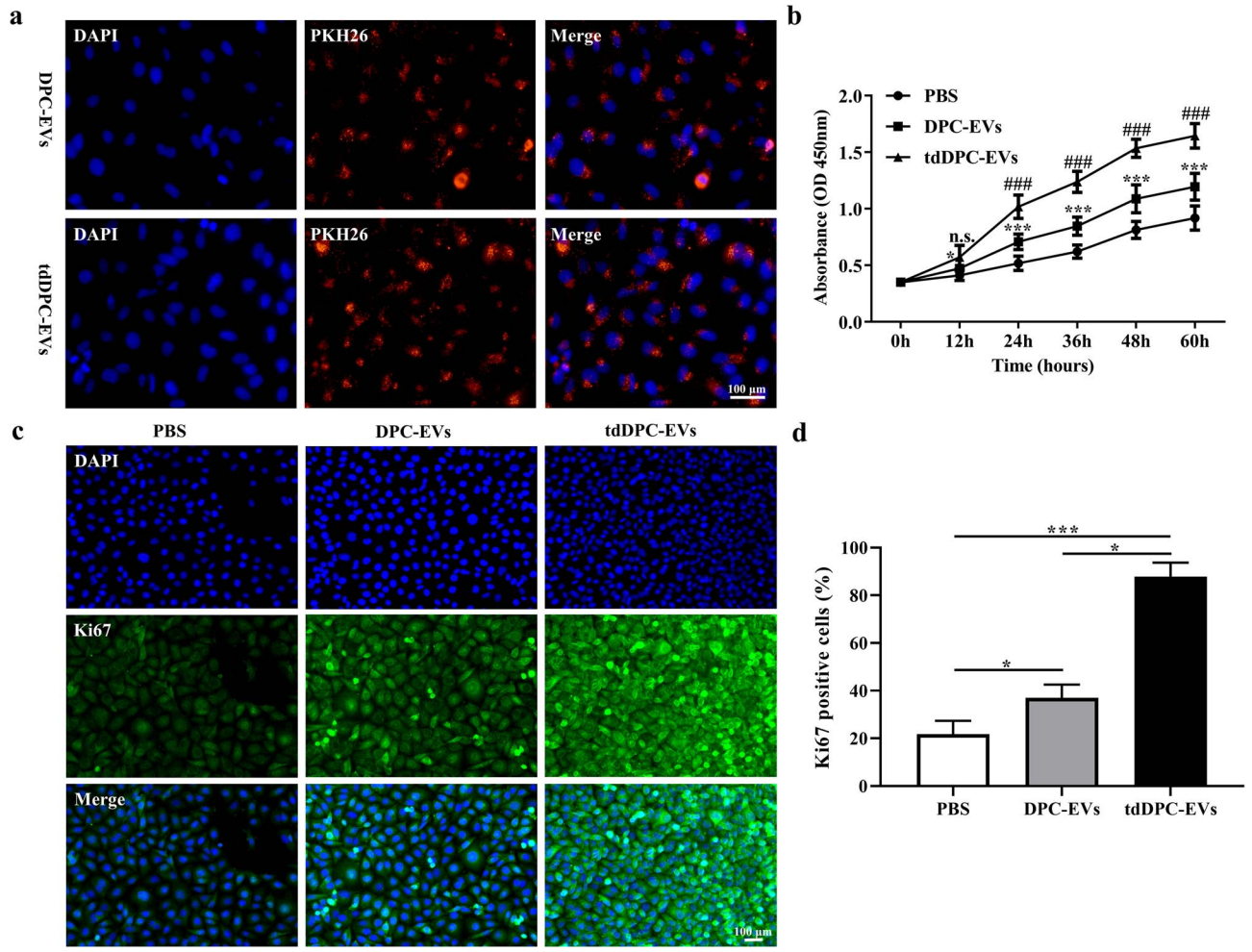

Figure 4. 3D dermal papilla cell extracellular vesicles (tdDPC-EVs) induced stronger promotion of human umbilical vein endothelial cell (HUVEC) proliferation than dermal papilla cell extracellular vesicles (DPC-EVs) and PBS. (**a**) Fluorescence microscopy analysis of PKH26-labeled tdDPC-EV internalization by HUVECs. (**b**) CCK-8 assays were performed to examine proliferation after treatment; n = 4, n.s. no statistical significance, $^{*}p < 0.05$ tdDPC-EVs *vs* PBS, $^{***}p < 0.001$ tdDPC-EVs *vs* PBS, $^{\#\#\#}p < 0.001$ tdDPC-EVs *vs* DPC-EVs. (**c**) Immunofluorescence staining for Ki67 in tdDPC-EVs-, DPC-EVs- and PBS-treated HUVECs. (**d**) Statistical results of Ki67-positive cells; n = 4, $^{*}p < 0.05$, $^{***}p < 0.001$. Scale bar: 100 μm. *DAPI* 4′,6-diamidino-2-phenylindole, *PBS* phosphate-buffered saline

identified, including 433 and 222 genes with up- and down-regulated expression, respectively (Figure 7a). DEG profiling showed that the expression of *KLF4* was upregulated in the tdDPC-EV group (Figure 7b). We previously confirmed that KLF4 could remarkably alleviate hypertrophic scar fibrosis as a pivotal transcription factor [35]. Thus, we considered whether KLF4 could regulate angiogenesis. Considering that the functional roles of KLF4 are based on its capacity to target downstream effectors, we performed conjoint bioinformatic analysis of the activity of KLF4 as a transcription factor, including the targeted relationship based on predicting binding sequences and correlated expression. Several DEGs were predicted as KLF4 targets, including a specific pro-angiogenic factor encoding *VEGFA* (Figure 7c). Altogether, the bioinformatic analysis results suggest that VEGFA may be a promising target of KLF4, through which tdDPC-EVs promotes angiogenesis in HUVECs.

tdDPC-EVs promote angiogenesis via KLF4-mediated upregulation of VEGFA expression

Based on the upregulation of *KLF4* expression detected via RNA-seq, we sought to determine whether tdDPC-EVs improved angiogenesis in the wound-healing process via KLF4/VEGFA signaling. First, the RNA-seq results were preliminarily verified using qRT-PCR and western blotting, and the results showed that *KLF4* and *VEGFA* expression exhibited identical upregulation patterns (Figure 8a–c). Meanwhile, we employed KLF4 shRNA to knockdown KLF4 expression (shKLF4) in HUVECs following treatment with tdDPC-EVs, and a KLF4-overexpressing vector to restore expression (Figure 8d). KLF4 knockdown hindered the pro-angiogenic effect of tdDPC-EVs on HUVECs (Figure 8e, f). Rescue-of-function experiments indicated that KLF4 over-expression rescued the inhibited pro-angiogenic capacity, accompanied by an accordant variation in VEGFA expression

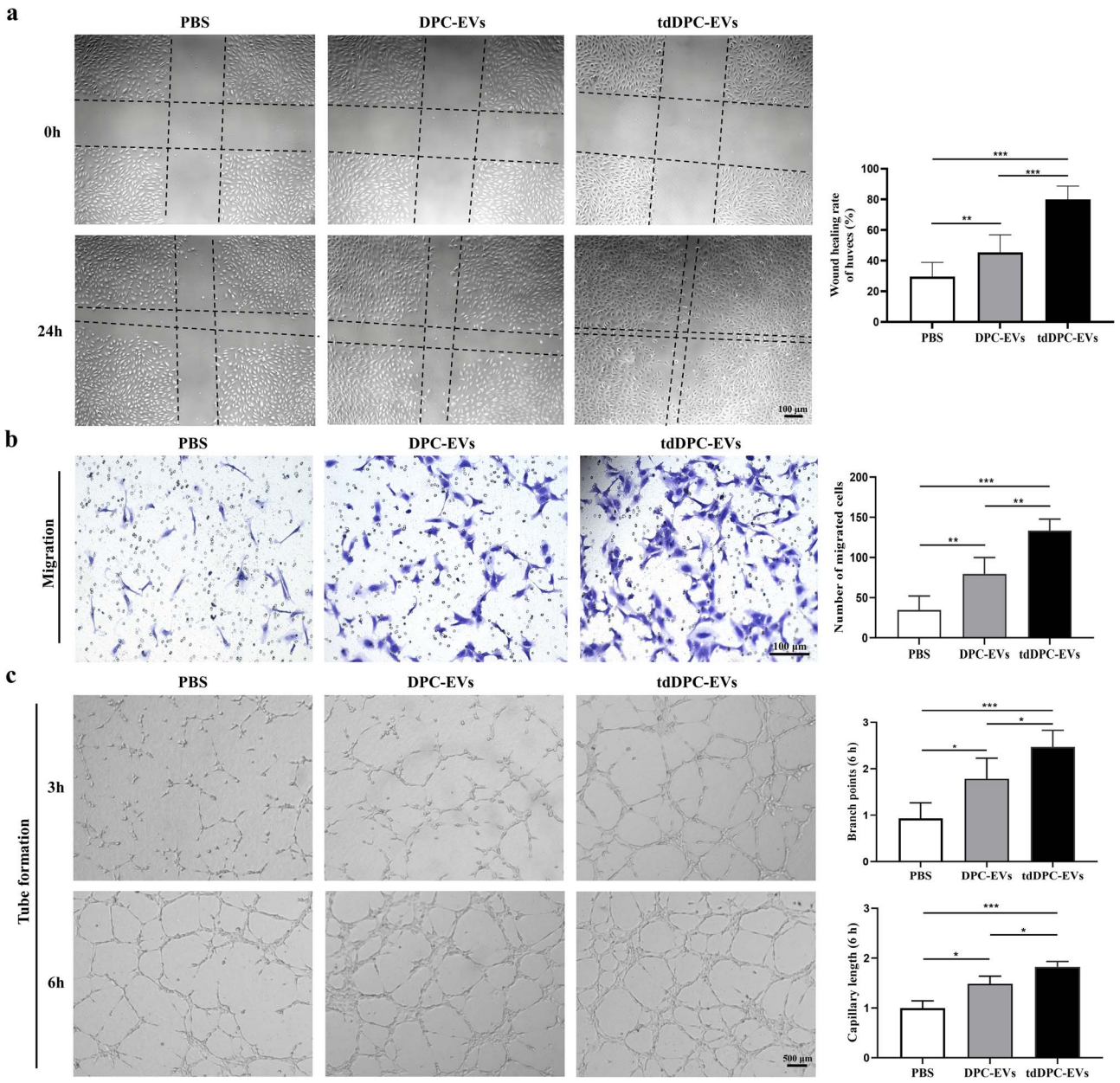

Figure 5. 3D dermal papilla cell extracellular vesicles (tdDPC-EVs) exert greater pro-angiogenic effects on human umbilical vein endothelial cells (HUVECs) than dermal papilla cell extracellular vesicles (DPC-EVs). Scratch-wound (**a**) and Transwell assays (**b**) were performed to evaluate the migration of HUVECs treated with DPC-EVs (10 μg/ml), tdDPC-EVs (10 μg/ml) or an equal volume of PBS. (**c**) DPC-EVs significantly increased the tube-formation ability of HUVECs, whilst tdDPC-EVs increased tube formation to a greater extent; *Scale bar: 100 & 500 μm,* $n=5$, $^{*}p<0.05$, $^{**}p<0.01$, $^{***}p<0.001$. *PBS* phosphate-buffered saline

(Figure 8e, f). The bioinformatics analysis revealed that the promoter region of the *VEGFA* gene (−801 to −812) contained a KLF4-binding sequence (5′-CTCCCCACCCGT-3′; Figure 8g). To further verify whether KLF4 activated VEGFA expression, we cloned the intact *VEGFA* promoter into luciferase constructs. The dual-luciferase reporter assay indicated that KLF4 could directly activate *VEGFA* transcription (Figure 8h). These observations suggested that KLF4/VEGFA signaling was required for the observed pro-angiogenic effects of tdDPC-EVs.

Beneficial component difference between DPC-EVs and tdDPC-EVs

RNA-seq was used to predict the difference in beneficial components between tdDPC-EVs and DPC-EVs. The Venn diagram shows that there were differences in miRNA expression between DPC-EVs and tdDPC-EVs, among which 217 miR had the same expression trend (Figure 9a). Compared with DPC-EVs, tdDPC-EVs contained more abundant miRNA. The results of differential miRNA analysis and the volcano plot showed that there were 123 significant differentially

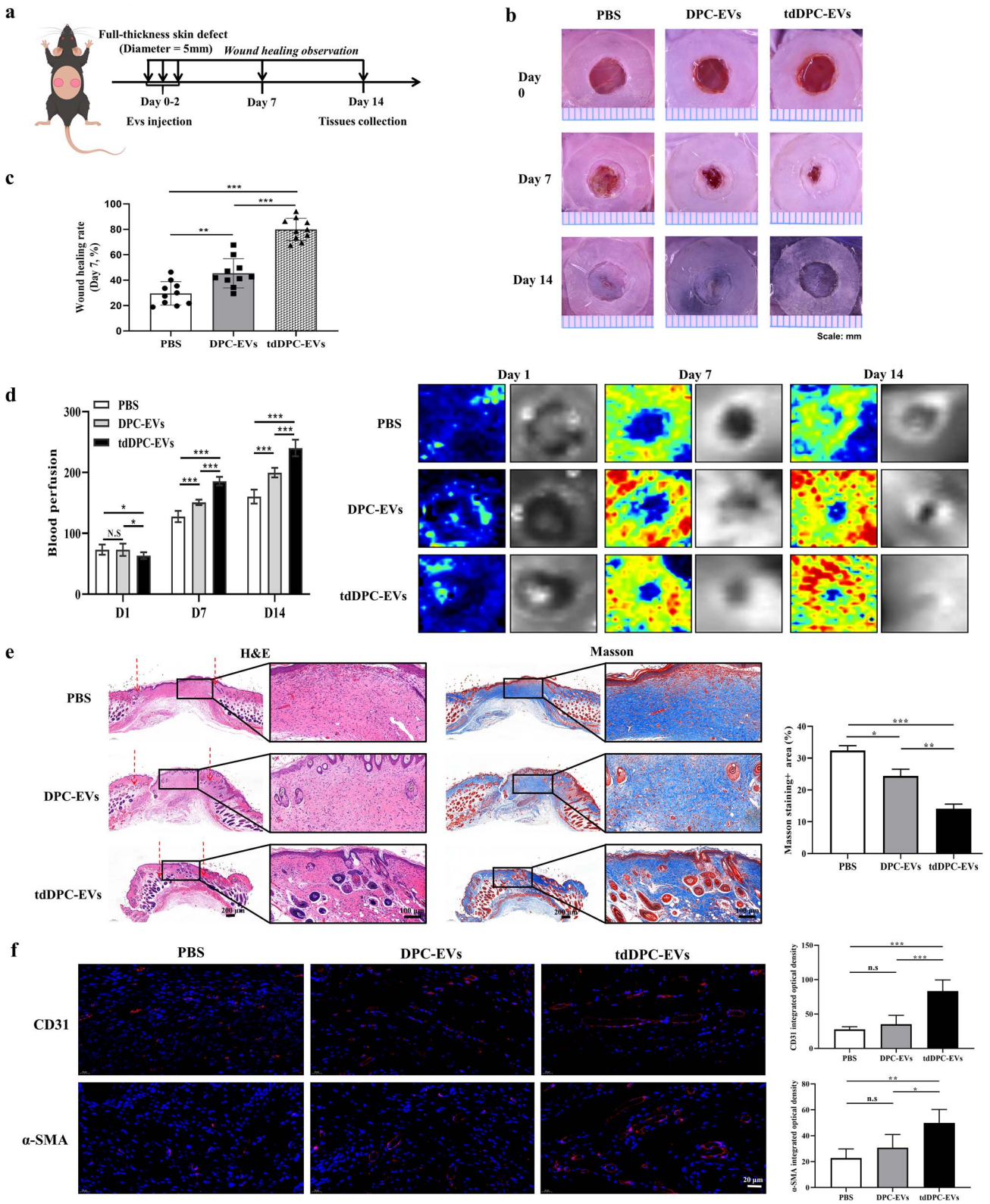

Figure 6. 3D dermal papilla cell extracellular vesicles (tdDPC-EVs) enhanced wound-healing efficiency and speed in mice. (**a**) Schematic diagram of the dermal papilla cell extracellular vesicle (DPC-EV) and tdDPC-EV treatment strategy for full-thickness skin defects in mice; n = 10. (**b**) Gross view of wounds treated with tdDPC-EVs, DPC-EVs or PBS. (**c**) Wound-healing rate under different treatments on day 7 after wound induction. (**d**) Doppler perfusion imaging was employed to detect wound blood perfusion. (**e**) H&E and Masson staining^{+} of wound tissues on day 14. The red arrow shows the dermis of the wound in H&E-stained tissues, and quantitative statistical analysis of Masson staining results was performed. Scale bar: 100 & 200 μm. (**f**) Immunofluorescence staining and quantitative statistics for CD31 and α-SMA staining on tissue sections. Scale bar: 20 μm. $^{*}p < 0.05$, $^{**}p < 0.01$, $^{***}p < 0.001$. *n.s.* no statistical significance, *PBS* phosphate-buffered saline, *H&E* hematoxylin and eosin, *α-SMA* α-Smooth muscle actin

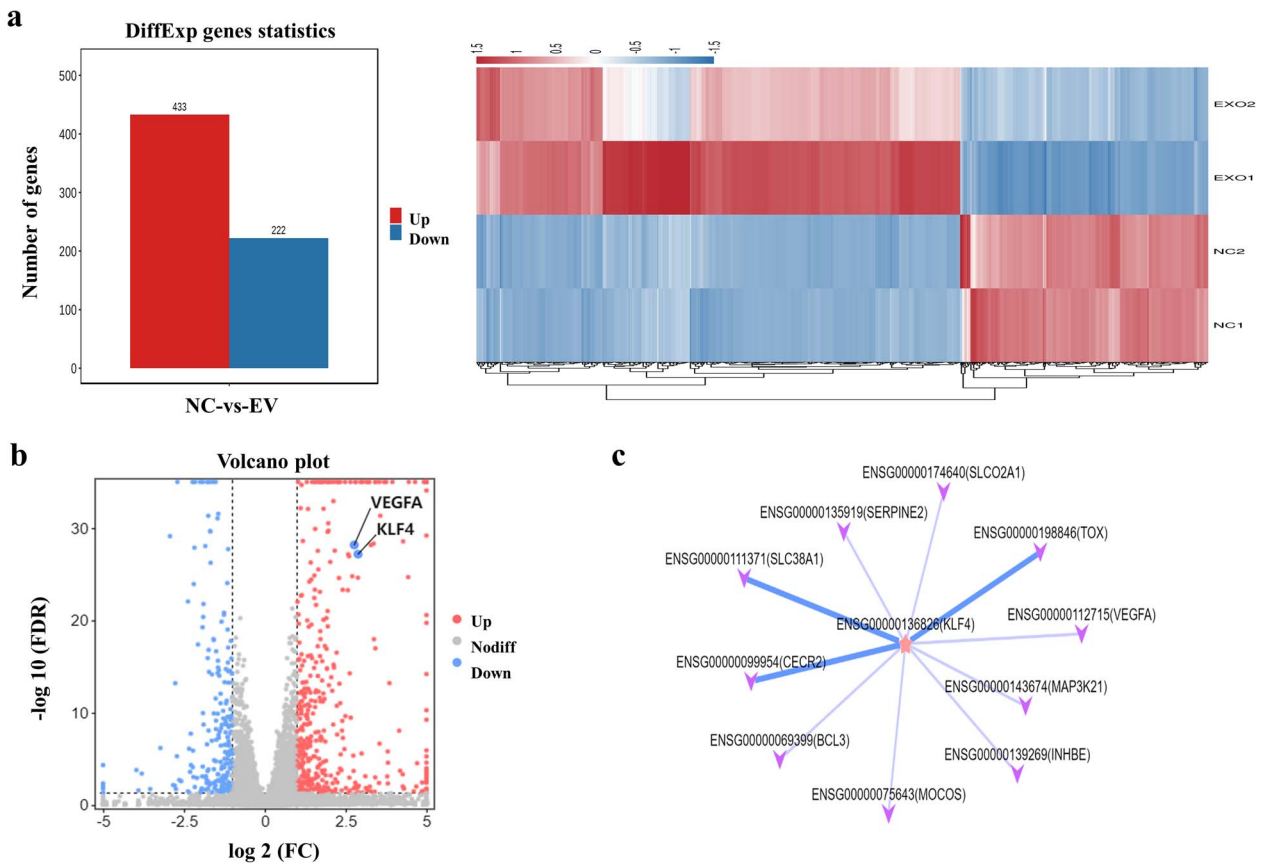

Figure 7. RNA-seq and bioinformatic analysis results suggest that Krüppel-like factor 4/vascular endothelial growth factor A (KLF4/VEGFA) mediates the pro-angiogenic effect of 3D dermal papilla cell extracellular vesicles (tdDPC-EVs). (**a**) Clustered heatmap based on differential gene expression (DiffExp) between the tdDPC-EV and control groups. (**b**) Volcano plot of *KLF4* and *VEGFA* in all differentially expressed genes. (**c**) Regulatory network of KLF4 as a transcription factor and its predicted target genes, including the angiogenic factor VEGFA. *FDR* false discovery rate, *KLF4* Krüppel-like factor 4, *VEGF* vascular endothelial growth factor

expressed miRNAs in DPC-EVs vs tdDPC-EVs, of which 85 had upregulated expression and 38 had downregulated expression (Figure 9b, c). Furthermore, the heatmap of differential miRNA expression also showed that there were significant differences in the regulation of angiogenesis-related miRNAs between DPC-EVs and tdDPC-EVs (Figure 9d). We found that, compared with DPC-EVs, the expression of miRNAs that promote endothelial cell proliferation, migration and angiogenesis were upregulated in tdDPC-EVs, while miRNAs that inhibit endothelial cell proliferation, migration and angiogenesis were downregulated.

Discussion

Wound healing is a complex process involving a sequence of well-characterized stages (coagulation, inflammation, angiogenesis and tissue remodeling), facilitated by intricate interactions between diverse cell types [36,37]. Despite the advances in wound-care strategies, therapeutic approaches for efficient and scar-free skin healing remain unsatisfactory [38]. Hence, developing an effective treatment that can accelerate and improve wound healing is imperative. Major advances in our knowledge of skin homeostasis have led to the identification of MSC-derived EVs as potential cell-free wound-healing therapeutic tools [4,39,40]. Increasing evidence has highlighted the value of HF-derived MSCs and their EVs for accelerating wound healing [41,42]. In the present study, we constructed tdDPCs through the SLF-3D culture of DPCs and utilized EVs from tdDPCs for wound treatment. A series of functional experiments evaluating the pro-angiogenic effects on HUVECs demonstrated that tdDPC-EVs drastically promoted wound healing-related angiogenesis through the KLF4-activated upregulation of VEGFA expression.

DPCs possess phenotypic plasticity during skin regeneration, which contributes to wound healing. Aamar *et al*. labeled the cells within the dermal papilla of mice that were homozygous for the Corin-CreRT2 allele and heterozygous for the r26EGFP reporter allele. They observed that GFP-labeled cells dissociated from follicle compartments and migrated toward the wound site on day 19 post-injury, indicating that DPCs contribute to wound healing [17]. Leirós *et al*. adopted DPCs as a dermal component in permanent composite skin with human HF stem cells in a single full-thickness skin wound and air–liquid interphase skin construct graft model in nude mice. They found that the presence of DPCs resulted in a better-stratified epidermis, favored the composite skin graft and increased the number of neovessels

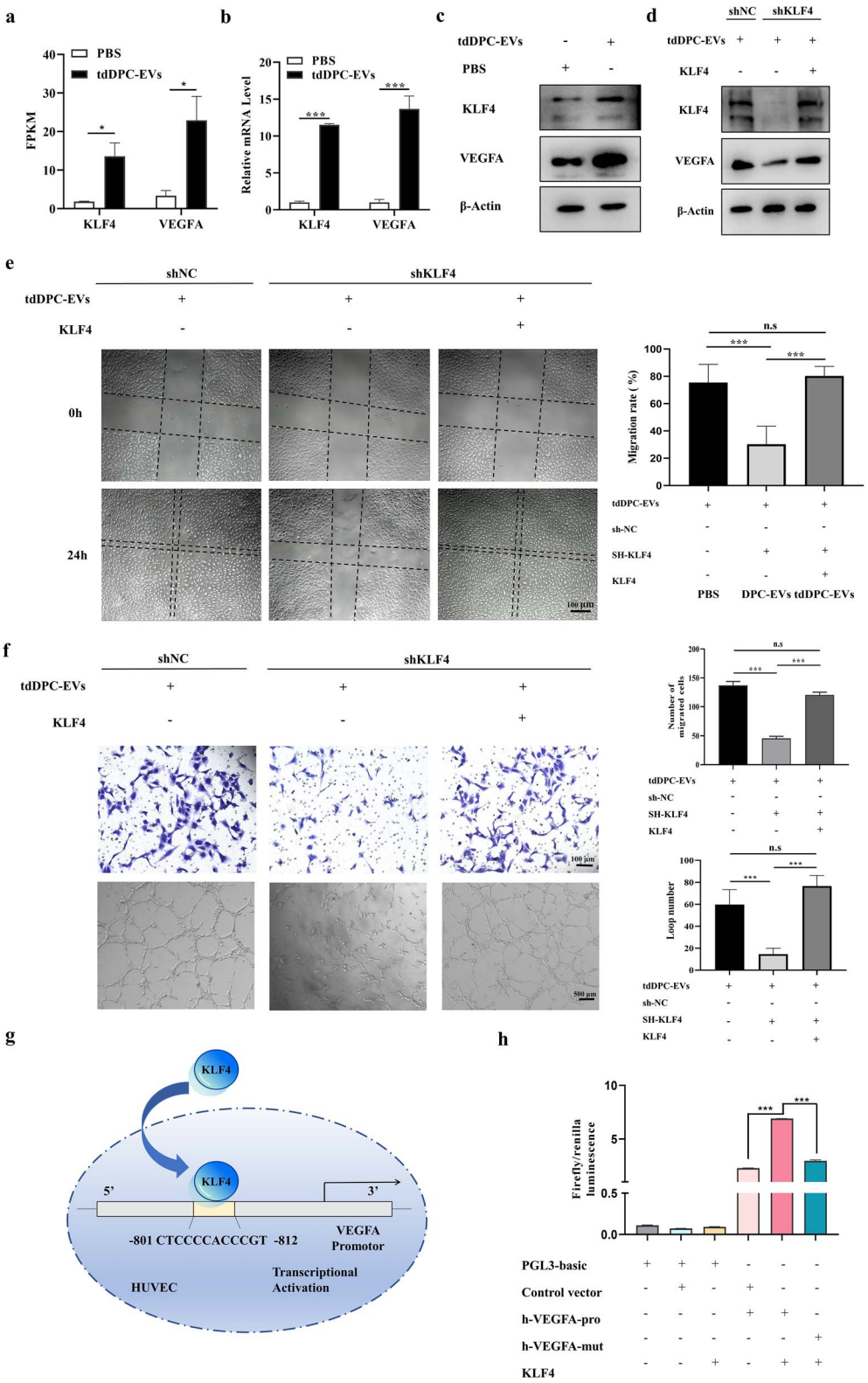

Figure 8. 3D dermal papilla cell extracellular vesicles (tdDPC-EVs) increased angiogenesis by promoting the Krüppel-like factor 4 (KLF4)-mediated activation of vascular endothelial growth factor A (VEGFA). (**a**) Reads per kilobase million (FPKM) of *KLF4* and *VEGFA*. (**b**, **c**) KLF4 and VEGFA expression in tdDPC-EV-treated HUVECs determined using qRT-PCR and western blotting. (**d**) KLF4 and VEGFA expression in tdDPC-EV-treated HUVECs with different KLF4 interference determined using western blotting. An shKLF4-resistant, reconstituted, KLF4-overexpressing vector, was used to restore KLF4 expression. (**e**) Scratch-wound and Transwell (**f**) assays revealed that KLF4 knockdown hindered the migration-promoting effect of tdDPC-EVs on HUVECs and reinforced that KLF4 rescued the effect; n = 5, scale bar: 100 μm. (f) KLF4 knockdown obstructed the increased tube-formation ability of tdDPC-EVs, while KLF4 restoration rescued the effect; n = 5, scale bar: 100 & 500 μm. (**g**) Schematic diagram of the *VEGFA* promoter. The yellow region is the putative KLF4-binding site. (**h**) Luciferase reporter gene analyses for the transcriptional activation of the *VEGFA* promoter by *KLF4*. $^{***}p < 0.001$. *n.s.* no statistical significance, *HUVECs* human umbilical vein endothelial cells, *PBS* phosphate-buffered saline

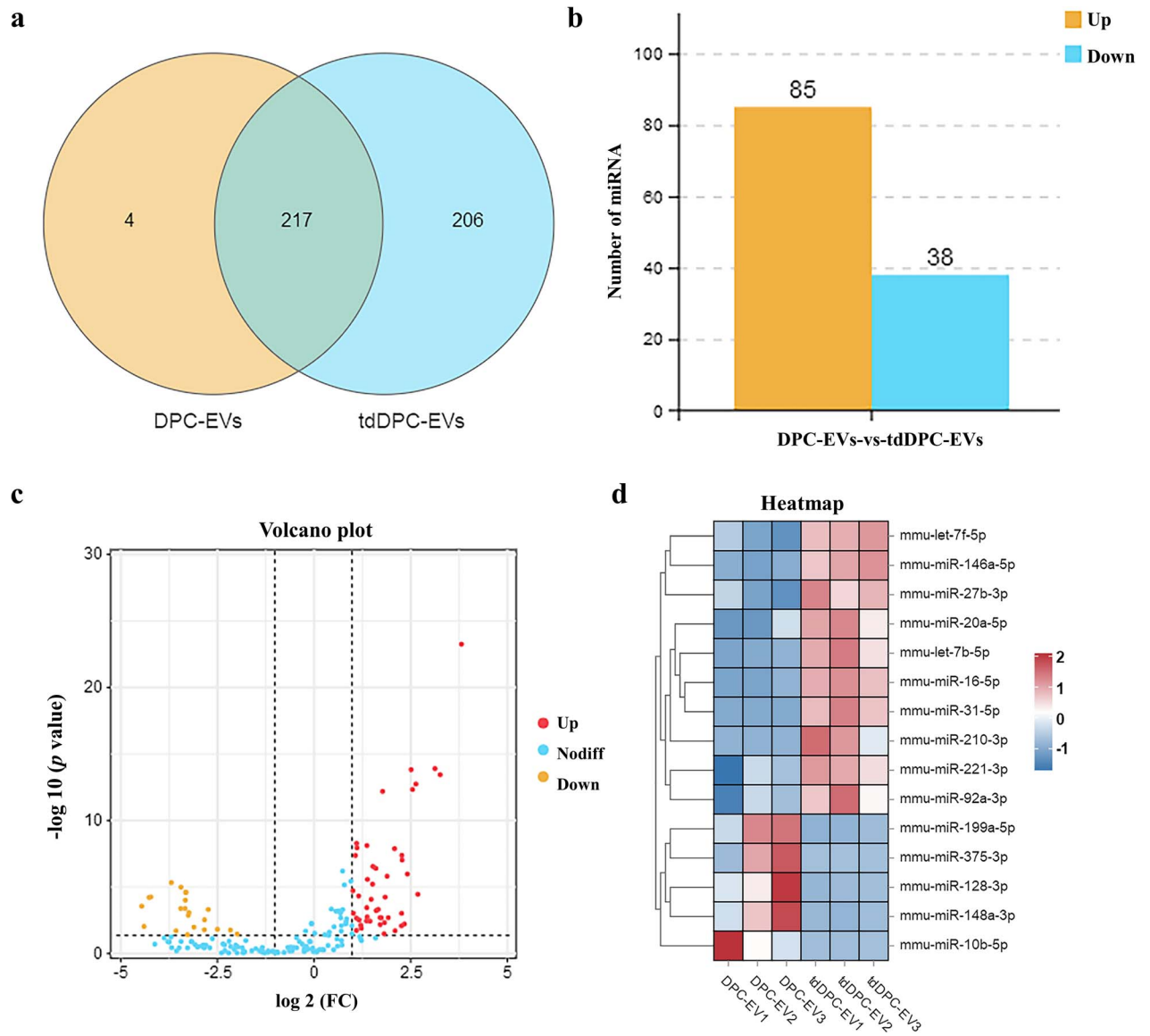

Figure 9. RNA-seq and bioinformatic analysis of dermal papilla cell extracellular vesicles (DPC-EVs) and 3D dermal papilla cell extracellular vesicles (tdDPC-EVs). (**a**) Venn diagram analysis of differentially expressed miRNAs between DPC-EVs and tdDPC-EVs. (**b**) Significant differences in miRNA expression between DPC-EVs and tdDPC-EVs. (**c**) Volcano plot to illustrate the number of significant miRNAs (DPC-EVs *vs* tdDPC-EVs). (**d**) Cluster heatmap of miRNA expression related to angiogenesis in DPC-EVs and tdDPC-EVs

[12]. These previous findings highlight the importance of DPCs for proper skin repair.

The plasticity and mobility of DPCs underpin their wound-healing properties, and the paracrine interactions between DPCs and various surrounding cell types are essential [14,43]. It is widely accepted that DPCs promote hair cycling through paracrine signaling, with secreted EVs predominantly mediating the associated intercellular interactions [44]. Existing research on DPC-EVs has mainly focused on regulating hair growth and has collectively established a positive role for DPC-EVs in hair regeneration [45]. For the first time, we used an SLF-3D culture system to culture a novel DPC spheroid, named tdDPC, which can improve the output and curative effect of EVs. Our findings demonstrated that DPC-EVs promoted the proliferation and migration of HUVECs. It has been shown that EVs isolated from HF-derived MSCs significantly enhance HUVEC proliferation, migration and angiogenesis *in vitro* [42]. Considering DPCs as specialized MSCs, our finding that DPC-EVs and tdDPC-EVs promote angiogenesis strongly supports the potential value of MSC-EVs in wound healing.

Previous studies have demonstrated that primary DPCs subjected to long-term traditional 2D culture possess many limitations, imposed by increased cell volume, accelerated cell senescence and reduced proliferation. Some studies concluded that isolated primary DPCs lose their hair-inducing potency when subjected to traditional culturing [46,47]. Hence, research efforts have been directed toward resolving the issue

of efficiently acquiring DPCs that harbor inductive activities. Various studies have confirmed that 3D spheroid cultures could restore the hair-inducing capacity of DPCs. It has been reported that DPC spheroids could exhibit superior hair growth-inducing capacity *in vivo*, unlike DPCs cultured on a flat, plastic surface, with the former positively influencing the local injection site as well as non-treated areas via paracrine signaling [15]. Kang *et al*. developed human DPC spheres using either a low cell-binding plate or a hydrocell plate that possessed hair-inducing abilities [48]. The researchers then extracted EVs from the spheres, which enhanced the proliferation of DPCs and outer root sheath cells via upregulating the expression of IGF-1, KGF and HGF growth factors, effectively inducing hair growth both *in vitro* and *in vivo*. However, no significant differences were observed between 2D DPC-EV and 3D DPC-EV treatments [49]. In the present study, we extracted DPC-EVs from 2D cultures and tdDPC-EVs from novel 3D spheroids and compared their efficacy in wound healing. We observed that tdDPC-EVs exhibited evident superiority with regard to wound-healing promotion compared with DPC-EVs. We suggest that the SLF-3D culture system containing growth factors and an adherent cell layer enhanced the biological activity of tdDPCs and gave rise to superior therapeutic efficacy of tdDPC-EVs in wound treatment. Hu *et al*. compared the effects of 2D DPC-EV and 3D DPC-EV treatments on mouse dorsal hair regeneration and observed that 3D DPC-EVs enhanced hair growth to a greater extent [15]. Zhang *et al*. previously demonstrated that the 3D culture of DPCs was more representative of *in vivo* conditions than 2D culture in the context of androgen-induced alopecia through co-culture with outer root sheath cells under dihydrotestosterone treatment *in vitro* [50]. In our SLF-3D culture approach, we exploited the inherent proliferative heterogeneity of DPCs and employed a small subset of highly proliferative populations to form tdDPCs on a specific matrix scaffold composed of adhered DPC subsets. The average particle size of tdDPC-EVs was about two times smaller than that of DPC-EVs, while the yield increased ∼6-fold, implying that tdDPC-EVs are more convenient for carrier encapsulation and offer greater application potential in drug delivery. In addition, we pioneered the use of EVs from this SLF-3D culture method in wound treatment. We confirmed that both the DPC-EV traditional monolayer and tdDPC-EV SLF-3D cultures could effectively promote wound healing, while tdDPC-EVs enhanced the speed and quality of wound healing to a greater extent. Considering the continuous production of tdDPC spheres from the original SLF-3D in parallel with secondary tdDPC sphere formation, there is no effective method to distinguish between these spheres. Thus, tdDPC-EVs could only be extracted by inoculating secondary spheres in ultra-low adhesion plates and collecting conditioned medium via conventional methods, highlighting the need for further optimization of 3D spheroid cultures.

In addition to optimizing cell culture conditions, pretreatment culture is also one of the key strategies to improve the function of MSCs [51]. Pretreatment of cells and their microenvironment can affect their content and the content of EVs. Common types of EV pretreatment include cytokines, hypoxia, drugs and physical intervention. Compared with untreated EVs, preconditioned EVs play an important role in tissue repair and have obvious advantages in regulating cell proliferation and apoptosis, inflammatory responses and angiogenesis [52–54]. Studies have shown that hypoxia can induce angiogenesis by enriching miRNAs in angiogenic EVs [55]. EVs obtained from MSCs pretreated with pioglitazone, atorvastatin or erythropoietin can significantly enhance the vitality of vascular endothelial cells in diabetic patients, promote collagen deposition and extracellular matrix remodeling, and simultaneously promote VEGF secretion and CD31 protein expression, thus promoting angiogenesis and wound healing in diabetic patients [56–58]. At present, the biological functions and characteristics of preconditioned source EVs have been studied and verified in the treatment of some diseases and achieved good results, suggesting that they may have broader applications in clinical settings for promoting wound healing. To develop an adaptive strategy to improve the yield and biological function of EVs, the specific mechanism and functional conditions of pretreatment need to be further studied.

It is widely recognized that angiogenesis, particularly microvasculature regrowth, is a prerequisite for efficient wound damage repair [59]. Wound healing generally comprises four stages (hemostasis, inflammation, proliferation and dermal remodeling), and angiogenic activity displays dynamic patterns throughout the entire process [60]. Neovascularization, especially rapid capillary proliferation, is a prominent feature following wound induction. Prior to the dermal remodeling stage, angiogenic processes establish a disorganized vascular network, leading to significant numbers of densely packed new blood vessels. As the wound healing transitions into the stage of dermal remodeling, vascular networks are characterized by vessel maturation, including capillary lumen occlusion, an apparent decrease in the number of capillaries and the appearance of larger, mature vessels with thickened walls [61]. Here, we observed that tdDPC-EVs more effectively enhanced wound blood perfusion than did DPC-EVs during wound healing *in vivo*. CD31 and α-SMA immunofluorescence analysis of wound skin tissues on day 14 revealed that tdDPC-EVs could promote vascular network maturation at a faster rate than did DPC-EVs or the control treatment. Moreover, a series of angiogenic assays confirmed the greater pro-angiogenic effects of tdDPC-EVs on HUVECs. Based on the above-described results, we speculate that tdDPC-EVs promote angiogenesis during the earlier healing phase, and thereafter, convert capillaries into larger, mature vessels in the remodeling phase.

To elucidate the specific molecular mechanisms underlying the ability of tdDPC-EVs to promote angiogenesis during wound healing, we employed RNA-seq to compare gene expression changes between tdDPC-EV- and PBS-treated HUVECs, which led to the identification of the transcription factor KLF4 as a differentially regulated gene. Silencing KLF4

compromised the observed pro-angiogenic effect of tdDPC-EVs on HUVECs, while subsequent overexpression rescued tdDPC-EV-induced angiogenesis. Thus, we demonstrated that tdDPC-EVs promote angiogenesis through the upregulation of KLF4 expression, consistent with the results of other studies highlighting the positive role of KLF4 in wound healing [62,63]. Based on the bioinformatic analysis results, we sought to explore the role of VEGFA as a direct transcriptional target of KLF4. VEGFA levels were upregulated in response to KLF4 overexpression under tdDPC-EV treatment. Furthermore, luciferase reporter assays confirmed the direct binding of KLF4 to the *VEGFA* promoter in HUVECs. Angiogenesis-related growth factors are essential for wound healing, and VEGFA plays a central role in the angiogenic process [64]. Consistent with our findings, KLF4 has been reported to positively regulate angiogenesis by transcriptionally upregulating *VEGF* expression in human retinal microvascular endothelial cells [65]. Cao *et al*. demonstrated that VEGFA could form a positive feedback loop with KLF4 to promote endometrial angiogenesis of human endometrial microvascular endothelial cells. They not only confirmed the positive transcriptional activation of *VEGFA* by KLF4 but also confirmed that VEGFA could, in turn, epigenetically regulate the transcriptional activity of *KLF4* [66]. In contrast, Boriushkin *et al*. found that KLF4 suppressed neovascular tuft formation and vaso-obliteration in an oxygen-induced retinopathy model [67]. These inconsistencies may be explained by the complexity of KLF4 regulatory circuits in different angiogenic processes. Our observations provide a basis for the pro-angiogenic role of the KLF4/VEGFA axis in the context of the wound-healing process. In addition, we carried out RNA-seq of DPC-EVs and tdDPC-EVs, and the results suggest that miRNA contained in tdDPC-EVs may play a key role in regulating wound healing. For example, the upregulated expression of let-7b-5p, miR-31-5p and miR-221-3p has been reported to promote the proliferation, migration and angiogenesis of endothelial cells in wound healing [56,68,69]. The downregulated expression of miR-199a-5p has been proved to inhibit angiogenesis [70]. In addition, the upregulated expression of miR-16-5p in tdDPC-EVs has been shown to accelerate wound healing of deep second-degree burns in mice by mediating keratinocyte migration in vesicles derived from pluripotent stem cells [71]. However, the specific miRNAs involved in tdDPC-EV regulation of the angiogenic effect of the KLF4/VEGFA axis in wound healing needs to be further explored. Taken together, we determined that KLF4/VEGFA signaling mediated tdDPC-EV-induced angiogenesis, thus enhancing wound-healing speed and quality.

Conclusions

In summary, our study suggests that tdDPCs have the capacity for efficient proliferation and stem cell differentiation, providing a new alternative cell source for EV extraction. Furthermore, we elucidated the potential therapeutic ability of tdDPC-EVs in wound healing; that is, tdDPC-EVs significantly improve wound healing via KLF4/VEGFA-driven angiogenesis and 3D culture can be utilized as an innovative optimization strategy for applying DPC-derived EVs for wound healing.

Abbreviations

ALP: Alkaline phosphatase; bFGF: Basic fibroblast growth factor; DEGs: Differentially expressed genes; DMEM: Dulbecco's modified Eagle's medium; DPCs: Dermal papilla cells; EGF: Epidermal growth factor; EVs: extracellular vesicles; FBS: Fetal bovine serum; FPKM: Fragments per kilobase of transcript per million mapped reads; H&E: Hematoxylin and eosin; HFs: Hair follicles; HUVECs: Human umbilical vein endothelial cells; IGF-1: Insulin-like growth factor 1; KLF4: Krüppel-like factor 4; LEF1: Lymphoid enhancer-binding factor 1; MSCs: Mesenchymal stem cells; PDGF: Platelet-derived growth factor; qRT-PCR: Quantitative reverse transcription-polymerase chain reaction; RNA-seq: RNA-sequencing; SLF-3D: Self-feeder 3D; tdDPCs: 3D-DPC spheroids; TEM: Transmission electron microscopy; VEGF: Vascular endothelial growth factor; α-SMA: α-Smooth muscle actin; HRP: Horseradish peroxidase; DAPI:4′,6-diamidino-2-phenylindole; PE: phycoerythrin; FITC: fluorescein isothiocyanate; ROI: return on investment; FDR: false discovery rate; BCA: bicinchoninic acid; miRNA: microRNA; miR: microRNA; FC: fold change; NC: negative control; ECL: enhanced chemiluminescence; shRNA: short hairpin RNA; HGF: hepatocyte growth factor; KGF: Keratinocyte growth factor.

Acknowledgments

We gratefully acknowledge Mr Tao Liu (Gene Denovo Biotechnology Co., Ltd, Guangzhou, China) for his assistance with the bioinformatics analysis in this manuscript. The diagrams in Graphical Abstract were modified from Servier Medical Art (https://smart.servier.com) under the CC BY 3.0 licence (https://creativecommons.org/licenses/by/3.0/). The DPCs diagram in Graphical Abstract were acquired from Figdraw (http://www.figdraw.com) (ID: POUOS22869 & ID: YSOUR72dd9). The authors thank all the other members in their laboratory for their insights and technical support.

Funding

This work was supported by the National Natural Science Foundation of China (No. 82272268) and the Industry-University-Research Innovation Fund of China (2021JH030).

Authors' contributions

HG, YSY, LL, and YWW designed the research; YWW, KS, YLS, PC, QYZ and BW performed the experiments; YWW, JZ, WFZ, YL, YC, and SHL performed statistical analysis; HZ, CLX, YTQ, CH purchased the reagents; YSY and YWW wrote the article. All authors read and approved the final manuscript.

Data availability

The datasets used and/or analyzed during the current study are available from the corresponding author upon reasonable request. The RNA-seq data used in this study have been deposited in the National Center for Biotechnology Information's Sequence Read Archive (https://www.ncbi.nlm.nih.gov/sra/PRJNA890242).

Ethics approval and consent to participate

Experimental protocols involving animals were approved by the Animal Care and Use Committee of Fourth Military Medical University.

Conflict of interests

None declared.

References

1. Werner S, Grose R. Regulation of wound healing by growth factors and cytokines. *Physiol Rev*. 2003;83:835–70.
2. Ju YK, Fang BR. Research advances on the mechanism of extracellular vesicles of adipose-derived mesenchymal stem cells in promoting wound angiogenesis. *Chin J Burns Wounds*. 2023;39:85–90.
3. Han C, Barakat M, DiPietro LA. Angiogenesis in wound repair: too much of a good thing? *Cold Spring Harb Perspect Biol*. 2022;14:a041225.
4. Wang M, Wu P, Huang J, Liu W, Qian H, Sun Y, *et al*. Skin cell-derived extracellular vesicles: a promising therapeutic strategy for cutaneous injury. Burns. *Trauma*. 2022;10:tkac037.
5. Wu P, Zhang B, Shi H, Qian H, Xu W. MSC-exosome: a novel cell-free therapy for cutaneous regeneration. *Cytotherapy*. 2018;20:291–301.
6. Gan Y, Wang H, Du L, Li K, Qu Q, Liu W, *et al*. Cellular heterogeneity facilitates the functional differences between hair follicle dermal sheath cells and dermal papilla cells: a new classification system for mesenchymal cells within the hair follicle niche. *Stem Cell Rev Rep*. 2022;18:2016–27.
7. Hagner A, Shin W, Sinha S, Alpaugh W, Workentine M, Abbasi S, *et al*. Transcriptional profiling of the adult hair follicle mesenchyme reveals R-spondin as a novel regulator of dermal progenitor function. *iScience*. 2020;23:101019.
8. Rezza A, Wang Z, Sennett R, Qiao W, Wang D, Heitman N, *et al*. Signaling networks among stem cell precursors, transit-amplifying progenitors, and their niche in developing hair follicles. *Cell Rep*. 2016;14:3001–18.
9. Greco V, Chen T, Rendl M, Schober M, Pasolli HA, Stokes N, *et al*. A two-step mechanism for stem cell activation during hair regeneration. *Cell Stem Cell*. 2009;4:155–69.
10. Clavel C, Grisanti L, Zemla R, Rezza A, Barros R, Sennett R, *et al*. Sox2 in the dermal papilla niche controls hair growth by fine-tuning BMP signaling in differentiating hair shaft progenitors. *Dev Cell*. 2012;23:981–94.
11. Gharzi A, Reynolds AJ, Jahoda CA. Plasticity of hair follicle dermal cells in wound healing and induction. *Exp Dermatol*. 2003;12:126–36.
12. Leirós GJ, Kusinsky AG, Drago H, Bossi S, Sturla F, Castellanos ML, *et al*. Balañá, dermal papilla cells improve the wound healing process and generate hair bud-like structures in grafted skin substitutes using hair follicle stem cells. *Stem Cells Transl Med*. 2014;3:1209–19.
13. Madaan A, Verma R, Singh AT, Jaggi M. Review of hair follicle dermal papilla cells as in vitro screening model for hair growth. *Int J Cosmet Sci*. 2018;40:429–50.
14. Bassino E, Gasparri F, Giannini V, Munaron L. Paracrine crosstalk between human hair follicle dermal papilla cells and microvascular endothelial cells. *Exp Dermatol*. 2015;24:388–90.
15. Hu S, Li Z, Lutz H, Huang K, Su T, Cores J, *et al*. Dermal exosomes containing miR-218-5p promote hair regeneration by regulating β-catenin signaling. *Sci Adv*. 2020;6:eaba1685.
16. Zhao B, Li J, Zhang X, Dai Y, Yang N, Bao Z, *et al*. Exosomal miRNA-181a-5p from the cells of the hair follicle dermal papilla promotes the hair follicle growth and development via the Wnt/β-catenin signaling pathway. *Int J Biol Macromol*. 2022;207:110–20.
17. Aamar E, Avigad Laron E, Asaad W, Harshuk-Shabso S, Enshell-Seijffers D. Hair-follicle mesenchymal stem cell activity during homeostasis and wound healing. *J Invest Dermatol*. 2021;141:2797–2807.e6.
18. Driskell RR, Clavel C, Rendl M, Watt FM. Hair follicle dermal papilla cells at a glance. *J Cell Sci*. 2011;124:1179–82.
19. Higgins CA, Chen JC, Cerise JE, Jahoda CA, Christiano AM. Microenvironmental reprogramming by three-dimensional culture enables dermal papilla cells to induce de novo human hair-follicle growth. *Proc Natl Acad Sci U S A*. 2013;110:19679–88.
20. Abreu CM, Cerqueira MT, Pirraco RP, Gasperini L, Reis RL, Marques AP. Rescuing key native traits in cultured dermal papilla cells for human hair regeneration. *J Adv Res*. 2020;30:103–12.
21. Abbott A. Cell culture: biology's new dimension. *Nature*. 2003;424:870–2.
22. Topouzi H, Logan NJ, Williams G, Higgins CA. Methods for the isolation and 3D culture of dermal papilla cells from human hair follicles. *Exp Dermatol*. 2017;26:491–6.
23. Osada A, Iwabuchi T, Kishimoto J, Hamazaki TS, Okochi H. Long-term culture of mouse vibrissal dermal papilla cells and de novo hair follicle induction. *Tissue Eng*. 2007;13:975–82.
24. Yuan X, Sun L, Jeske R, Nkosi D, York SB, Liu Y, *et al*. Engineering extracellular vesicles by three-dimensional dynamic culture of human mesenchymal stem cells. *J Extracell Vesicles*. 2022;11:e12235.
25. Jalilian E, Massoumi H, Bigit B, Amin S, Katz EA, Guaiquil VH, *et al*. Bone marrow mesenchymal stromal cells in a 3D system produce higher concentration of extracellular vesicles (EVs) with increased complexity and enhanced neuronal growth properties. *Stem Cell Res Ther*. 2022;13:425.
26. Habanjar O, Diab-Assaf M, Caldefie-Chezet F, Delort L. 3D cell culture systems: tumor application, advantages, and disadvantages. *Int J Mol Sci*. 2021;22:12200.
27. Fitzgerald SJ, Cobb JS, Janorkar AV. Comparison of the formation, adipogenic maturation, and retention of human adipose-derived stem cell spheroids in scaffold-free culture techniques. *J Biomed Mater Res B Appl Biomater*. 2020;108:3022–32.
28. Ryu NE, Lee SH, Park H. Spheroid culture system methods and applications for mesenchymal stem cells. *Cell*. 2019;8:1620.
29. Luo L, Zhang W, Chen W, Fu X, Wang X, Xu R, *et al*. Based on a self-feeder layer, a novel 3D culture model of human ADSCs facilitates trans-differentiation of the spheroid cells into neural

progenitor-like cells using siEID3 with a Laminin/poly-d-lysine matrix. *Cell*. 2021;10:493.
30. Luo L, Zhang W, Wang J, Zhao M, Shen K, Jia Y, *et al.* A novel 3D culture model of human ASCs reduces cell death in spheroid Cores and maintains inner cell proliferation compared with a nonadherent 3D culture. *Front Cell Dev Biol.* 2021;9:737275.
31. Gledhill K, Gardner A, Jahoda CA. Isolation and establishment of hair follicle dermal papilla cell cultures. *Methods Mol Biol*. 2013;989:285–92.
32. Jahoda CA, Whitehouse J, Reynolds AJ, Hole N. Hair follicle dermal cells differentiate into adipogenic and osteogenic lineages. *Exp Dermatol*. 2003;12:849–59.
33. Hoogduijn MJ, Gorjup E, Genever PG. Comparative characterization of hair follicle dermal stem cells and bone marrow mesenchymal stem cells. *Stem Cells Dev*. 2006;15:49–60.
34. Love MI, Huber W, Anders S. Moderated estimation of fold change and dispersion for RNA-seq data with DESeq2. *Genome Biol*. 2014;15:550.
35. Wang J, Zhao M, Zhang H, Yang F, Luo L, Shen K, *et al.* KLF4 alleviates hypertrophic scar fibrosis by directly activating BMP4 transcription. *Int J Biol Sci*. 2022;18:3324–36.
36. Brazil JC, Quiros M, Nusrat A, Parkos CA. Innate immune cell-epithelial crosstalk during wound repair. *J Clin Invest*. 2019;129:2983–93.
37. Rodrigues M, Kosaric N, Bonham CA, Gurtner GC. Wound healing: a cellular perspective. *Physiol Rev*. 2019;99:665–706.
38. Willyard C. Unlocking the secrets of scar-free skin healing. *Nature*. 2018;563:S86–8.
39. Narauskaitė D, Vydmantaitė G, Rusteikaitė J, Sampath R, Rudaitytė A, Stašytė G, *et al.* Extracellular vesicles in skin wound healing. *Pharmaceuticals (Basel)*. 2021;14:811.
40. Wang T, Jian Z, Baskys A, Yang J, Li J, Guo H, *et al.* MSC-derived exosomes protect against oxidative stress-induced skin injury via adaptive regulation of the NRF2 defense system. *Biomaterials*. 2020;257:120264.
41. Ma D, Kua JE, Lim WK, Lee ST, Chua AW. In vitro characterization of human hair follicle dermal sheath mesenchymal stromal cells and their potential in enhancing diabetic wound healing. *Cytotherapy*. 2015;17:1036–51.
42. Las Heras K, Royo F, Garcia-Vallicrosa C, Igartua M, Santos-Vizcaino E, Falcon-Perez JM, *et al.* Extracellular vesicles from hair follicle-derived mesenchymal stromal cells: isolation, characterization and therapeutic potential for chronic wound healing. *Stem Cell Res Ther*. 2022;13:147.
43. Robinson M, Reynolds AJ, Jahoda CA. Hair cycle stage of the mouse vibrissa follicle determines subsequent fiber growth and follicle behavior in vitro. *J Invest Dermatol.* 1997;108:495–500.
44. Chen Y, Huang J, Chen R, Yang L, Wang J, Liu B, *et al.* Sustained release of dermal papilla-derived extracellular vesicles from injectable microgel promotes hair growth. *Theranostics*. 2020;10:1454–78.
45. Gangadaran P, Rajendran RL, Kwack MH, Jeyaraman M, Hong CM, Sung YK, *et al.* Application of cell-derived extracellular vesicles and engineered Nanovesicles for hair growth: from mechanisms to therapeutics. *Front Cell Dev Biol*. 2022;10:963278.
46. Yang CC, Cotsarelis G. Review of hair follicle dermal cells. *J Dermatol Sci*. 2010;57:2–11.
47. Ohyama M, Zheng Y, Paus R, Stenn KS. The mesenchymal component of hair follicle neogenesis: background, methods and molecular characterization. *Exp Dermatol*. 2010;19:89–99.
48. Kang BM, Kwack MH, Kim MK, Kim JC, Sung YK. Sphere formation increases the ability of cultured human dermal papilla cells to induce hair follicles from mouse epidermal cells in a reconstitution assay. *J Invest Dermatol*. 2012;132:237–9.
49. Kwack MH, Seo CH, Gangadaran P, Ahn BC, Kim MK, Kim JC, *et al.* Exosomes derived from human dermal papilla cells promote hair growth in cultured human hair follicles and augment the hair-inductive capacity of cultured dermal papilla spheres. *Exp Dermatol*. 2019;28:854–7.
50. Zhang Y, Huang J, Fu D, Liu Z, Wang H, Wang J, *et al.* Transcriptome analysis reveals an inhibitory effect of Dihydrotestosterone-treated 2D- and 3D-cultured dermal papilla cells on hair follicle growth. *Front Cell Dev Biol*. 2021;9:724310.
51. Phan J, Kumar P, Hao D, Gao K, Farmer D, Wang A. Engineering mesenchymal stem cells to improve their exosome efficacy and yield for cell-free therapy. *J Extracell Vesicles*. 2018;7:1522236.
52. Huang P, Wang L, Li Q, Tian X, Xu J, Xu J, *et al.* Atorvastatin enhances the therapeutic efficacy of mesenchymal stem cells-derived exosomes in acute myocardial infarction via up-regulating long non-coding RNA H19. *Cardiovasc Res*. 2020;116:353–67.
53. Chen H, Xia W, Hou M. LncRNA-NEAT1 from the competing endogenous RNA network promotes cardioprotective efficacy of mesenchymal stem cell-derived exosomes induced by macrophage migration inhibitory factor via the miR-142-3p/FOXO1 signaling pathway. *Stem Cell Res Ther*. 2020;11:31.
54. Liu W, Yu M, Xie D, Wang L, Ye C, Zhu Q, *et al.* Melatonin-stimulated MSC-derived exosomes improve diabetic wound healing through regulating macrophage M1 and M2 polarization by targeting the PTEN/AKT pathway. *Stem Cell Res Ther*. 2020;11:259.
55. Namazi H, Mohit E, Namazi I, Rajabi S, Samadian A, Hajizadeh-Saffar E, *et al.* Exosomes secreted by hypoxic cardiosphere-derived cells enhance tube formation and increase pro-angiogenic miRNA. *J Cell Biochem*. 2018;119:4150–60.
56. Yu M, Liu W, Li J, Lu J, Lu H, Jia W, *et al.* Exosomes derived from atorvastatin-pretreated MSC accelerate diabetic wound repair by enhancing angiogenesis via AKT/eNOS pathway. *Stem Cell Res Ther*. 2020;11:350.
57. Hu Y, Tao R, Chen L, *et al.* Exosomes derived from pioglitazone-pretreated MSCs accelerate diabetic wound healing through enhancing angiogenesis. *J Nanobiotechnology*. 2021;19:150.
58. Lu H, Wu X, Wang Z, *et al.* Erythropoietin-activated mesenchymal stem cells promote healing ulcers by improving microenvironment. *J Surg Res*. 2016;205:464–73.
59. Okonkwo UA, DiPietro LA. Diabetes and wound angiogenesis. *Int J Mol Sci*. 2017;18:1419.
60. Broughton G, 2nd, Janis JE, Attinger CE. Wound healing: an overview. *Plast Reconstr Surg*. 2006;117:1e-S-32e-S.
61. Veith AP, Henderson K, Spencer A, Sligar AD, Baker AB. Therapeutic strategies for enhancing angiogenesis in wound healing. *Adv Drug Deliv Rev*. 2019;146:97–125.
62. Ou L, Shi Y, Dong W, Liu C, Schmidt TJ, Nagarkatti P, *et al.* Kruppel-like factor KLF4 facilitates cutaneous wound healing by promoting fibrocyte generation from myeloid-derived suppressor cells. *J Invest Dermatol.* 2015;135:1425–34.

63. Yang X, Mathis BJ, Huang Y, Li W, Shi Y. KLF4 promotes diabetic chronic wound healing by suppressing Th17 cell differentiation in an MDSC-dependent manner. *J Diabetes Res*. 2021;2021:7945117.
64. Weng T, Wang J, Yang M, Zhang W, Wu P, You C, *et al*. Nanomaterials for the delivery of bioactive factors to enhance angiogenesis of dermal substitutes during wound healing. *Burns Trauma*. 2022;10:tkab049. https://doi.org/10.1093/burnst/tkab049.
65. Wang Y, Yang C, Gu Q, Sims M, Gu W, Pfeffer LM, *et al*. KLF4 promotes angiogenesis by activating VEGF Signaling in human retinal microvascular endothelial cells. *PLoS One*. 2015;10:e0130341.
66. Cao C, Zhou Y, Zhang Y, *et al*. GCN5 participates in KLF4-VEGFA feedback to promote endometrial angiogenesis. *iScience*. 2022;25:104509.
67. Boriushkin E, Zhang H, Becker M, Peachey J, Shatat MA, Adams RH, *et al*. Kruppel-like factor 4 regulates developmental angiogenesis through disruption of the RBP-J-NICD-MAML complex in intron 3 of Dll4. *Angiogenesis*. 2019;22:295–309.
68. Yan C, Chen J, Wang C, Yuan M, Kang Y, Wu Z, *et al*. Milk exosomes-mediated miR-31-5p delivery accelerates diabetic wound healing through promoting angiogenesis. *Drug Deliv*. 2022;29:214–28.
69. Giotta Lucifero A, Luzzi S. Brain AVMs-related microRNAs: machine learning algorithm for expression profiles of target genes. *Brain Sci*. 2022;12:1628.
70. Heuslein JL, Gorick CM, McDonnell SP, Song J, Annex BH, Price RJ. Exposure of endothelium to biomimetic flow waveforms yields identification of miR-199a-5p as a potent regulator of Arteriogenesis. *Mol Ther Nucleic Acids*. 2018;12:829–44.
71. Yan Y, Wu R, Bo Y, Zhang M, Chen Y, Wang X, *et al*. Induced pluripotent stem cells-derived microvesicles accelerate deep second-degree burn wound healing in mice through miR-16-5p-mediated promotion of keratinocytes migration. *Theranostics*. 2020;10:9970–83.